

This article presents a nice and detailed investigation of the photolysis, ozonolysis and OH-reaction of a conjugated carbonyl nitrate produced in the oxidation of isoprene by NO<sub>3</sub> radical. The topic is of great importance to atmospheric chemistry since the formation and fate of organic nitrates play an outstanding role through their influence on the budget of NO<sub>x</sub> over forested areas. The methods are appropriate and the analysis is sound (with some minor reservations as explained further below). The article is also very well-written, very clear, and appropriately illustrated. Although the focus is on a specific compound which in itself plays probably only a very minor role in the atmosphere, the results regarding the rates of photolysis and reaction with OH and O<sub>3</sub> are very likely valid to a broader class of compounds which are important intermediates in the oxidation of isoprene and (no doubt) many other compounds.

### **General comment**

Among several interesting findings, this study provides sound evidence that the interaction between the two chromophores in a nitrooxy enal enhances its absorption cross section as well as its photolysis quantum yield, so much so that photolysis is their dominant sink in atmospheric conditions around mid-day. This view was proposed as a general trait for alpha- and beta-nitrooxy carbonyls (Muller et al., 2014), based on the laboratory observation of strongly enhanced photolysis rates (compared to nonconjugated carbonyls) for several keto-nitrates (Suarez-Bertoa et al., 2012) and for several compounds including ethanal nitrate, the simplest aldehyde nitrate (Muller et al., 2014). That this enhancement also exists for nitrooxy enals (or enones) was previously proposed, but lacked experimental proof, which is provided here. The conjugated nature of the compound under consideration is very important given the distinct features of photolysis parameters of enals or enones compared to other carbonyls, and I think this aspect should be acknowledged in the manuscript. Because of very low quantum yields (ca. 0.004), the photolysis of MACR and MVK is almost negligible in spite of their very high cross sections above 300 nm. The presence of the nitrate group is found to increase the quantum yield by two orders of magnitude, to a value of the order of unity (0.28-0.48 in this study). On top of that, the cross sections are also enhanced, as nicely shown in this work. Overall, the presence of the ONO<sub>2</sub> group has a much more dramatic impact for the photolysis rates of enals (or enones) than for other carbonyls. For this reason, I recommend that the studied compound should be referred to as an enal in the title and in the abstract.

We have changed to refer to this compound as “isoprene nitrooxy enal”, or “nitrooxy enal”, in the title, abstract and the rest of the manuscript.

In addition, the article presents an experimental determination of the OH- and O<sub>3</sub>- reaction rates of the nitrooxy enal, thereby enabling the estimation of the relative contribution of photolysis and reaction with OH and O<sub>3</sub> to the total photochemical sink of this compound. Photolysis is found to be generally dominant during the day. The further degradation mechanism following photolysis or reaction with OH is also explored, and yields of different products are derived. Photolysis is believed to proceed in part C2 by O–NO<sub>2</sub> dissociation, as proposed in Muller et al. (2014), and for some part by C–CHO scission. Interpretation of the CIMS measurements and the derivation of yields is helped by kinetic modelling to account for the losses of the main observed products. The only reservation I have concerns the choice of photolysis rates for those products in this analysis

(see further below). But this is only a minor issue which should not affect the main conclusions of the study. I therefore recommend publication in ACP, after the authors take the above considerations into account, and address the following comments.

### **Minor comments**

lines 71-78: The interaction between chromophores in nitrooxy carbonyls (i.e. also aldehydes) was found to enhance not only the cross sections but also the quantum yields (Muller et al., 2014). The combined effects on cross sections and quantum yields were observed for ethanal nitrate and for the sum of methyl vinyl ketone nitrate and methacrolein nitrate (MVKNO<sub>3</sub> + MACRNO<sub>3</sub>) of which the measured temporal evolution in the experiment of Paulot et al. (2009) provided constraints on the photolysis parameters. A quantum yield of the order of unity was also proposed for the major nitrooxy enal produced in the oxidation of isoprene by NO<sub>3</sub>. Its estimated photolysis rate was  $5.6 \times 10^{-4} \text{ s}^{-1}$  for a solar zenith angle of 30 degrees, assuming a unity quantum yield and using the cross sections of MACR. As a consequence, photolysis was estimated to outrun OH-oxidation in atmospheric conditions.

On lines 73-80 of the revised manuscript, we have added more clarification on the results reported by the Muller et al. (2014) study, to indicate that the interaction between chromophores can enhance both cross section and quantum yield.

line 168: The error bar for the wall loss rate constant appears somewhat optimistic in view of the scatter shown on Fig. 6. How was it derived?

The reported error is the standard error (s) of the coefficient. For clarification, we now report the result with 95% confidence interval, using  $t_{(N-2)} * s$  on lines 215-216.

line 175: "... cis isomer was present". I guess you mean "... was formed from the trans isomer", correct?

We have re-worded the reasoning for this part on line 226-238.

Figure 7. The caption should tell that the cross sections of the nitrate were obtained in acetonitrile.

We have included this information in the caption.

line 239: Is the factor 1.7 an average weighted by the irradiance spectrum?

The factor 1.7 is not a weighted average. It is calculated as the average ratio of gas-phase cross section divided by condensed-phase cross section at each wavelength. This is clarified on lines 296-298.

lines 393: Using the photorate of the 4,1-carbonyl nitrate to represent the photolysis loss of ethanal nitrate and the MVK nitrate is not appropriate as those compounds are not conjugated and their absorption cross sections are expected to be much lower in the relevant wavelength range (300-400 nm). For MVKNO<sub>3</sub>, I recommend to use the cross sections of 3-nitrooxy-2-butanone which are known from Barnes et al. (1993), and a quantum yield of unity since this choice led to best results for MVKNO<sub>3</sub>+MACRNO<sub>3</sub> evolution in Muller et al. (2014). For ethanal nitrate, the cross sections shown in Fig. 2 in Muller et al. (2014) could be used, as it was also found to give good results against Paulot et al. This update should decrease the calculated photolysis frequencies, especially for MVKNO<sub>3</sub>. Note that the OH-reaction rate of MVKNO<sub>3</sub> according to Kwok and Atkinson (1995) is  $1.3 \times 10^{-12} \text{ cm}^3 \text{ molec}^{-1} \text{ s}^{-1}$ , which might not be entirely negligible.

We calculated the photolysis frequency of 3-nitrooxy-2-butanone using the cross section reported by Barnes et al. (1993) and a unity quantum yield. The result,  $4.5\text{E-}6 \text{ s}^{-1}$  is used as a surrogate for the photolysis frequency of MVKNO<sub>3</sub>. We calculated the MVKNO<sub>3</sub> + OH rate constant as  $1.78\text{E-}12 \text{ cm}^3 \text{ molec}^{-1} \text{ s}^{-1}$ , based on Kwok and Atkinson (1995). We corrected the MVKNO<sub>3</sub> yield using these updated loss rates on lines 468-481.

We calculated that the photolysis frequency for ethanal nitrate is  $1.69\text{E-}5 \text{ s}^{-1}$ , using the cross section recommended by Muller et al (2014) and a unity quantum yield. This information is added on lines 464-466.

line 494: As far as photolysis is concerned, I don't really see why unsaturated ketones would be much different from unsaturated aldehydes. The absorption cross sections and quantum yields of MVK and MACR are very similar.

The unsaturated ketones and aldehydes are expected to have similar photochemical properties, given their similar structures, but the ketones may not be as reactive to OH as the aldehydes. We have made the clarification on lines 583-587.

### Technical corrections

line 106 "derived"

line 213: "were known" -> "are known"

line 214: "we calculated" -> "we calculate"

line 220: "introduced" → "introduce"

line 226: "we calculated that lambda0 was..." → "we calculate that lambda should be..."

line 273: "multiplying by..."

The above corrections have been made.

## References

Barnes, I., Becker, K. H., and Zhu, T.: Near UV absorption spectra and photolysis products of difunctional organic nitrates: Possible importance as NO<sub>x</sub> reservoirs, *Journal of Atmospheric Chemistry*, 17, 353-373, 10.1007/bf00696854, 1993.

Kwok, E. S. C., and Atkinson, R.: Estimation of hydroxyl radical reaction rate constants for gas-phase organic compounds using a structure-reactivity relationship: An update, *Atmospheric Environment*, 29, 1685-1695, [http://dx.doi.org/10.1016/1352-2310\(95\)00069-B](http://dx.doi.org/10.1016/1352-2310(95)00069-B), 1995.

Müller, J. F., Peeters, J., and Stavrou, T.: Fast photolysis of carbonyl nitrates from isoprene, *Atmospheric Chemistry and Physics*, 14, 2497-2508, 10.5194/acp-14-2497-2014, 2014.

The manuscript, "Photochemical degradation of isoprene-derived 4,1-carbonyl nitrate" by Xiong et al. reports on the photolysis rate of the trans-4-1 carbonyl nitrate derived in the atmosphere from the NO<sub>3</sub> radical oxidation of isoprene. The manuscript is well written and describes a great deal of well-thought-out work. The main implication of this work is that this conformer of isoprene carbonyl nitrate will have a short lifetime in the atmosphere due mainly to photolysis, with non-negligible contribution from OH oxidation. The work also identifies some of the major byproducts of OH oxidation and photolysis of this compound, thereby improving our understanding of isoprene photochemistry. The work should be published in ACP with a few minor clarifications.

Minor questions/comments/suggestions: I disagree with the "double" and "single" exponential discussion (lines 175-178). That a double exponential will be observed if large amounts of cis is present is unconvincing without additional information and likely cannot be concluded without knowing the isomerization rate. What is the chamber residence time? A cis-trans equilibrium at some point will be reached. If the rate at which this occurs is instantaneous (or at least much faster than residence time), a single exponential will always be observed because the CIMS only ever sees a mixture of the two isomers. Would you expect a significant difference in the photolysis rate of cis versus trans? If not, does it matter which isomer you are measuring? All that matters for this part of the experiment is the decay rate. If photo lifetime of cis versus trans is very different, you would have to qualify that the  $1.3 \times 10^{-5}$  sec<sup>-1</sup> rate is some average of the two isomers.

The chamber is operated in a static rather than dynamic mode. The duration of each experiment is about 3 hours. If a cis-trans equilibrium is established instantaneously, a single exponential will be observed. However, we don't expect the cis and trans isomer to differ in photolysis frequency, given they both have the nitrooxy enal structure. Therefore, the measured decay rate should represent the photolysis frequency of the trans precursor in the reaction chamber. We have added this discussion to lines 226-238.

It would be helpful to know which compounds whose structures are drawn in figures 10 and 15, as well as those boxed in figures 11 and 12 are observed by both GC and CIMS. The CIMS captures signal at nominal masses, therefore, to infer not only molecular composition (C<sub>x</sub>H<sub>y</sub>O<sub>z</sub>) but molecular structure (i.e. identifying functional groups) would impart a certain amount of uncertainty. If only the CIMS without GC is used to infer a compound identity (such as dinitrates which I imagine do not survive GC column), this is worth clarifying. Also, how well can you distinguish MVK nitrate from MACR nitrate with GC /CIMS?

The compounds that were observed by both GC and CIMS are now indicated in blue. The structures proposed in figures 10-12 and 15-16 are inferred based on nominal masses. We have added this information to the captions of these graphs.

We are unclear how well the GC/CIMS can distinguish MVK nitrate from MACR nitrate. For this work, we do not expect to have MACR nitrate in the system, because the nitrooxy enal has a secondary carbon at its C3 position, and the OH oxidation reaction cannot add a functional group at this position while still maintaining it as a secondary carbon as in MACR nitrate. Therefore, we infer m/z 276 to be MVK nitrate. We have added this discussion to lines 409-412.

Given CIMS observations of boxed compounds in figures 12 and 16, can you infer branching ratios of OH oxidation paths (a versus b in figure 12) and the two photolysis paths (figure 16).

The branching ratios for the OH oxidation cannot be obtained because the products from H-abstraction pathway were not quantified. For the OH addition pathway, we did quantify two of the products. However, ethanal nitrate is produced from both H abstraction and OH addition pathways (including both (a) and (b) pathways). MVK nitrate is produced in pathway (b) only, but it has ethanal nitrate as byproduct (along with C5 dinitrate), which makes it impossible to determine the branching ratio for pathway (b). We have added this discussion to lines 491-497.

For photolysis pathways, we cannot determine the branching ratio because the photolysis products were identified, but not quantified. This is clarified on lines 549-552.

How were the spectra in figure 3 obtained? Are they of three different samples, one containing pure carbonyl nitrate in solvent, the second pure MACR, and the third pure isopropyl nitrate? If the spectra are of one mixture containing all three compounds, how were the spectra distinguished or attributed to a particular compound?

The spectra were obtained with three different samples, each one containing one pure solute in the acetonitrile solvent. This is clarified on line 99-100.

Is each a simulated or calculated spectrum from the observed (the sum of the three spectra shown in figure 3). This needs to be better explained, in particular, for the discussion on lines 142 to 165. This discussion tries to establish that the excitation features of carbonyl nitrate is well understood, that the one near 255 nm is from the nitrate group C2 and the one near 330 nm is from the aldehyde group. However, there are some aspects of this discussion that are difficult to follow, hence, the argument is not as convincing as can be. For instance, figure 3 shows isopropyl nitrate along with MACR and carbonyl nitrate, whereas figure 4 shows n-butyl nitrate. Explain why the combination of these 3 compounds was chosen for this part of the study...similarity in structure, overlapping functional groups, etc. Figure 4 and 5 involve calculations...why not include isopropyl nitrate as well? It would make comparison simpler and argument more convincing.

The calculation was performed for each spectrum separately. In Fig. 3, we compared isopropyl nitrate and MACR with isoprene nitrooxy enal, because MACR has the enal structure, and isopropyl nitrate has the nitrooxy group, and the combination of these two compounds resembles the nitrooxy enal studied in this work. This explanation was added to lines 102-105 of the revised manuscript.

To better compare the measured UV spectra with the calculated spectra, we have now added calculations for isopropyl nitrate in section 3.2 and 4.1 of the revised manuscript.

Figure 4 is described as an absorption spectrum. But it looks very different from figure 3. Figure 4 looks more like band strength or absorption lines. Is it possible to simulate actual absorption spectra (one for MACR, one for carbonyl nitrate, one for n-butyl nitrate) given data shown in figure 4 under conditions similar to those in figure 3 and compare that result to figure 3? Would provide stronger support to TDDFT calculation.

Fig. 4 shows the theoretical gas phase absorption spectra of the nitrooxy enal, MACR, isopropyl nitrate, and n-butyl nitrate. To accurately capture the broadening of these lines in TDDFT, it is required to consider the effect of the chromophore's vibrational degrees of freedom and/or to include a condensed phase environment that surrounds the chromophore. However, explicit modeling of broadening either due to vibronic interactions or solvent effects is computationally challenging. We believe the analysis of this kind is beyond the scope of the present work. It is also possible to artificially broaden stick spectra with Gaussian or Lorentzian envelopes, to represent collision broadening. However, we do not think that such artificial broadening would provide any additional information, while the presented stick theoretical spectra provide adequate support for our arguments. This discussion is added to lines 165-170.

Lines 142-144, reads as if authors are saying there is a transition for n-butyl nitrate near 330 nm when there is not. Please re-word.

We have re-worded the sentence to refer the 330 nm transition as a transition for the nitrooxy enal only on line 180-182.

Lines 148-149..."...Earth's surface..." what is the significance of this statement? Figure 5 and lines 159-165. What is the relevance of including the excitation feature near 210 nm (figure 4) when there is no experimental data (figure 3) to compare against. This spectral region is also "beyond atmospheric relevance" as authors note.

The theoretical calculations suggest that the nitrooxy group has an electronic transition at 210 nm and 255 nm, but both wavelengths are outside the solar radiation spectrum near the surface. Therefore, we speculate that the isoprene nitrooxy enal absorbs photons primarily through the transition of the enal chromophore, instead of the nitrooxy functionality, and the dissociation of the O-NO<sub>2</sub> bond likely results from intramolecular energy redistribution. This discussion is added to line 207-212.

Including those transitions gives a clear picture of how the theoretical spectrum of the nitrooxy enal is a function of both nitrooxy absorption and absorption of the enal group, through the comparison with the absorption of the alkyl nitrates and MACR. While though they might not seem directly relevant to the experimental data, they show internal consistency of the simulated spectra. This discussion is further clarified on line 198-200.

Figure 1. Is the reaction between the NO<sub>3</sub> radical and nitroxy peroxy radical the only route to the alkoxy radical, hence carbonyl nitrate? Isn't reaction with RO<sub>2</sub> more likely than NO<sub>3</sub> to generate the alkoxy given abundance of RO<sub>2</sub> in most BVOC rich region? At the very least, RO<sub>2</sub> should be included. Rollins et al 2009 ACP ([www.atmos-chemphys.net/9/6685/2009/](http://www.atmos-chemphys.net/9/6685/2009/)).

We have now included RO<sub>2</sub> as a second reactant to form nitrooxy alkoxy radicals in Fig. 1.

Application to field observation was demonstrated in figure 9. Out of curiosity, is there direct observation of isoprene carbonyl nitrate from the field using CIMS+GC? Spectrum or chromatogram or time series or diel average? How abundant is isoprene carbonyl nitrate considering it is produced at night when loss rate is presumably slow? How well can the CIMS distinguish C<sub>5</sub>H<sub>7</sub>NO<sub>4</sub> from potential interference due to the isotope of the signal at m/z 271. Do you have carbonyl nitrate + NO<sub>3</sub> oxidation results, similar to those of OH and photolysis shown here? These would be nice additions to this work, but perhaps saving for separate manuscript.

To date there is no report on field observations of isoprene carbonyl nitrates using CIMS or GC method. One of the challenges for this type of measurement might be that when iodide-based CIMS is used, the isoprene nitrooxy enal can react with iodide and form NO<sub>3</sub><sup>-</sup>, instead of nitrate-iodide cluster, and the nitrooxy enal could be detected as NO<sub>3</sub> and N<sub>2</sub>O<sub>5</sub> radicals. In addition, iodide-based CIMS is most sensitive to species with acidic hydrogens, which the enal nitrate does not have. Brown et al. (2009) observed NO<sub>3</sub> + isoprene chemistry in Northeast US in the 2004 NEAQS study, and they estimated that the total concentrations of the isoprene-derived nitrate could reach 500 ppt. The carbonyl nitrates are expected to contribute a significant fraction to the total organic nitrates estimated by Brown et al. (2009), but the exact amount cannot be obtained without direct measurement of the carbonyl nitrates. This discussion is added to lines 434-440.

Our CIMS has unit mass resolution. For this work, we used pure isoprene nitrooxy enal as the precursor, which did not introduce much interference at m/z 271. This is clarified on lines 122-124.

Since this work is focused on the photochemistry of the nitrooxy enal, which describes the loss-dominant processes after sunrise, we did not include experiments concerning NO<sub>3</sub> oxidation. This is clarified on lines 116-118 of the revised manuscript.

Figure 4. Many have a difficult time distinguishing red from blue. May help to choose different color scheme. Also, are vertical lines necessary to show this data? The three lines at 210 nm are difficult to distinguish from one another. Perhaps use markers instead? Also, change "1×10<sup>exponent</sup>" to just "10<sup>exponent</sup>"

Fig. 4 was updated including the changes suggested by the reviewer.



The wall loss rate constant is fairly high compared to the photolysis rate constant. What is the residence time in the 5.2 m long tubing? Is laminar flow maintained? Also, curious if heating the inlet to 50 degC can induce cis-trans isomerization.

The wall loss and photolysis rate constants were obtained with repeated experiments. The radiation inside the chamber is approximately 10% of solar radiation. Therefore, our photolysis rate constant is small, making the wall loss rate constant high compared with photolysis frequency. This information is added to line 218-220.

The residence time in the tubing is around 5 s, and laminar flow is maintained. We have conducted inlet tests for the heated tubing, and we do not expect significant isomerization inside our sampling line. This information is added to line 125-131.

Line 235. Why is there no gas phase spectrum? Is it technically challenging? If so, it would be helpful for community to know.

We were concerned about potentially large wall loss of the organic nitrate inside a small UV cell. Hence, the measurements were performed with nitrate solutions. This is clarified on line 100-102.

## Reference

Brown, S. S., deGouw, J. A., Warneke, C., Ryerson, T. B., Dubé, W. P., Atlas, E., Weber, R. J., Peltier, R. E., Neuman, J. A., Roberts, J. M., Swanson, A., Flocke, F., McKeen, S. A., Brioude, J., Sommariva, R., Trainer, M., Fehsenfeld, F. C., and Ravishankara, A. R.: Nocturnal isoprene oxidation over the Northeast United States in summer and its impact on reactive nitrogen partitioning and secondary organic aerosol, *Atmos. Chem. Phys.*, 9, 3027-3042, 10.5194/acp-9-3027-2009, 2009.

# 1 Photochemical Degradation of Isoprene-derived **4,1-Carbonyl** 2 **Nitrate**4,1-Nitrooxy Enal

3  
4 F. Xiong<sup>1</sup>, C. H. Borca<sup>1</sup>, L. V. Slipchenko<sup>1</sup> and P. B. Shepson<sup>1,2</sup>

5 [1] Department of Chemistry, Purdue University, West Lafayette, IN

6 [2] Department of Earth, Atmospheric and Planetary Sciences, Purdue University, West Lafayette,  
7 IN

8 Correspondence to: P. B. Shepson ([pshepson@purdue.edu](mailto:pshepson@purdue.edu))

## 9 **Abstract**

10 In isoprene-impacted environments, carbonyl nitrates are produced from NO<sub>3</sub>-initiated isoprene  
11 oxidation, which constitutes a potentially important NO<sub>x</sub> reservoir. To better understand the fate  
12 of isoprene carbonyl nitrates, we synthesized a model compound, *trans*-4-nitrooxy-2-methyl-2-  
13 buten-1-al (4,1-isoprene carbonyl nitrate, or 4,1-isoprene nitrooxy enal) and investigated its  
14 photochemical degradation process. The measured OH and O<sub>3</sub> oxidation rate constants (298 K) for  
15 this ~~carbonyl nitrate~~nitrooxy enal are  $4.1(\pm 0.7) \times 10^{-11} \text{ cm}^3 \text{ molecules}^{-1} \text{ s}^{-1}$  and  $4.4(\pm 0.3) \times 10^{-18} \text{ cm}^3$   
16  $\text{molecules}^{-1} \text{ s}^{-1}$ , respectively. ~~Its~~The UV absorption spectrum ~~of the carbonyl nitrate~~ was  
17 determined, and the result is consistent with TDDFT calculations. Based on its UV absorption  
18 cross section and photolysis frequency in a reaction chamber, we estimate that the ambient  
19 photolysis frequency for this compound is  $3.1(\pm 0.8) \times 10^{-4} \text{ s}^{-1}$  for a solar zenith angle (SZA) of 45°.   
20 The fast photolysis rate and high reactivity toward OH lead to a lifetime of less than one hour for  
21 the ~~carbonyl nitrate~~isoprene nitrooxy enal, with photolysis being a dominant daytime sink. The  
22 nitrate products derived from the OH oxidation and the photolysis of the ~~isoprene-nitrooxy~~  
23 ~~enal~~carbonyl nitrate were identified with an iodide-based chemical ionization mass spectrometer  
24 (CIMS). For the OH oxidation reaction, we quantified the yields of two nitrate products, methyl  
25 vinyl ketone (MVK) nitrate and ethanal nitrate, which together contributed to 3736(±5)% of the  
26 first-generation products.

## 27 1 Introduction

28 Over the past century, tropospheric background ozone concentrations have increased from around  
29 20 ppb to ~40 ppb, with urban-impacted concentrations often rising to 60-100 ppb (Parrish et al.,  
30 2014; Vingarzan, 2004), posing harmful effects on human health and crop yields (Lefohn and  
31 Foley, 1993; Lippmann, 1989). Tropospheric ozone is catalytically produced in the chemical  
32 reactions of nitrogen oxides ( $\text{NO}_x \equiv \text{NO} + \text{NO}_2$ ) and volatile organic compounds (VOCs) (Haagen-  
33 Smit, 1952).  $\text{NO}_2$  photolysis forms ozone (Blacet, 1952), and the ozone production rate is  
34 enhanced when the  $\text{NO-NO}_2\text{-O}_3$  cycle is coupled with the oxidation of VOCs (Chameides et al.,  
35 1988; Chameides and Walker, 1973; Chameides et al., 1992). When  $\text{NO}_x$  is incorporated into  
36 organic molecules and forms organic nitrates ( $\text{RONO}_2$ ), however, ozone formation is suppressed  
37 (Roberts, 1990). Organic nitrates are a temporary  $\text{NO}_x$  reservoir. Degradation of organic nitrates  
38 can release  $\text{NO}_2$  back into the atmosphere (Aschmann et al., 2011), and thus facilitate ozone  
39 production. Organic nitrates in the gas phase can also adsorb onto atmospheric aerosols, followed  
40 by condensed-phase hydrolysis (Rindelaub et al., 2015). This process removes the reactive  
41 nitrogen from the atmosphere permanently, as the nitrooxy group is turned-converted into the non-  
42 volatile  $\text{NO}_3^-$  ion (Darer et al., 2011; Hu et al., 2011). The relative importance of these parallel  
43 nitrate sinks affects the availability of  $\text{NO}_x$  and the ozone production rate in the troposphere.  
44 Therefore, detailed understanding of the loss mechanisms of organic nitrates is crucial to  
45 understanding the dynamics of ground-level ozone formation.

46 Modeling studies suggest that isoprene-derived organic nitrates have substantial influence on the  
47  $\text{NO}_x$  cycle and tropospheric  $\text{O}_3$  production (Horowitz et al., 2007; Mao et al., 2013; Paulot et al.,  
48 2012; Wu et al., 2007). During the daytime, isoprene is lost rapidly to OH oxidation, forming  
49 organic nitrates through the  $\text{RO}_2 + \text{NO}$  reaction, with a yield of 7-14% (Lockwood et al., 2010;  
50 Patchen et al., 2007; Paulot et al., 2009; Sprengnether et al., 2002; Tuazon and Atkinson, 1990;  
51 Xiong et al., 2015). At night, reaction with  $\text{NO}_3$  is a significant removal pathway for isoprene  
52 (Brown et al., 2009; Starn et al., 1998), and organic nitrates constitute 65-70% of the oxidation  
53 products (Perring et al., 2009; Rollins et al., 2009). While  $\text{NO}_3$ -initiated isoprene oxidation  
54 contributes to a small fraction of isoprene loss, this reaction pathway could generate approximately  
55 half of the isoprene-derived organic nitrates on a regional scale, due to its large nitrate yield  
56 (Horowitz et al., 2007; Xie et al., 2013).

57 Fig.1 shows the formation pathways of organic nitrate products from NO<sub>3</sub>-initiated oxidation of  
58 isoprene, including hydroperoxy nitrate, carbonyl nitrate and hydroxy nitrate. Reactions for only  
59 one of the nitrooxy peroxy radicals are shown for brevity. The hydroxy nitrates can be also formed  
60 in the OH-initiated isoprene oxidation reactions, and their production and degradation have been  
61 studied extensively in both laboratory and field studies (Chen et al., 1998; Giacomelli et al., 2005;  
62 Grossenbacher et al., 2004; Jacobs et al., 2014; Lee et al., 2014b; Lockwood et al., 2010; Patchen  
63 et al., 2007; Paulot et al., 2009; Sprengnether et al., 2002; Tuazon and Atkinson, 1990; Xiong et  
64 al., 2015). For the hydroperoxy nitrates, Schwantes et al. (2015) investigated their production from  
65 the RO<sub>2</sub> + HO<sub>2</sub> reaction and identified the nitrooxy hydroxyepoxide product from the OH oxidation  
66 of the isoprene hydroperoxy nitrate. For the isoprene carbonyl nitrates, their formation has been  
67 quantified in an experimental study (Kwan et al., 2012), but their sinks and fate can only be inferred  
68 from analog molecules, such as nitrooxy ketones, due to lack of direct studies on these specific  
69 compounds. Suarez-Bertoa et al. (2012) conducted kinetics experiments on three synthesized  
70 saturated nitrooxy ketones, and their results indicate that photolysis is the dominant sink for these  
71 nitrate compounds. By comparing the published UV absorption spectra of  $\alpha$ -nitrooxy ketones with  
72 the UV spectra of the mono-functional nitrates and ketones, Müller et al. (2014) suggested that the  
73 nitrooxy ketones have enhanced absorption cross sections, due to the interaction between the –  
74 C=O and the –ONO<sub>2</sub> chromophores. In addition, near-unit photolysis quantum yields for  $\alpha$ -  
75 nitrooxy acetone and 3-nitrooxy-2-butanone were inferred by Müller et al. (2014), based on the  
76 photolysis frequencies determined by Suarez-Bertoa et al. (2012) and known absorption cross  
77 sections (Barnes et al.). The enhanced absorption cross sections and quantum yields of carbonyl  
78 nitrates resulting from chromophore interactions lead to fast photolysis rates that are more  
79 consistent with the loss rates constrained by the measured temporal profiles of carbonyl nitrates in  
80 an isoprene oxidation experiment performed by Paulot et al. (2009) (Müller et al., 2014), ~~which~~  
81 can facilitate the dissociation of the O–NO<sub>2</sub> bond. Like the ~~nitrooxy ketones~~ carbonyl nitrates  
82 discussed by Suarez-Bertoa et al. (2012) and Müller et al. (2014), some of the carbonyl nitrate  
83 isomers derived from NO<sub>3</sub> + isoprene oxidation ~~has~~ have a conjugated chromophore, –C=C–C=O  
84 (enal), at the  $\beta$  position of the nitrate group, which may enhance the UV absorption cross section  
85 of the molecule and facilitate its photolytic dissociation. However, since the five-carbon isoprene  
86 carbonyl nitrate (nitrooxy enal) (Fig. 1) is unsaturated, it is also expected to be lost rapidly to OH  
87 oxidation. To date, the relative importance of the individual photochemical sinks for the

88 unsaturated carbonyl nitrates is still unclear. To answer this question, we synthesized a model  
89 compound for the five-carbon isoprene carbonyl nitrates, and investigated its photochemical  
90 reactivities and fate.

## 91 2 Synthesis and characterization

92 A model compound, ~~4,1 isoprene carbonyl nitrate~~ (*trans*-2-methyl-4-nitrooxy-2-buten-1-al (4,1-  
93 isoprene nitrooxy enal) was synthesized following the reaction scheme in Fig. 2. The nitrate was  
94 prepared by reacting AgNO<sub>3</sub> with the corresponding bromide (*trans*-4-bromo-2-methyl-2-buten-  
95 1-al) (Ferris et al., 1953), which was synthesized following Gray (1981). The <sup>1</sup>H and <sup>13</sup>C NMR  
96 spectra of the synthesized product are shown in Fig. S1 and Fig. S2. Its IR absorption spectrum is  
97 shown in Fig. S3.

98 Shown in Fig. 3 are the UV absorption cross sections for the ~~carbonyl nitrate~~nitrooxy enal,  
99 methacrolein (MACR) and isopropyl nitrate. Each spectrum was obtained using a solution that  
100 contained one single pure analyte in acetonitrile solvent. Only solution-phase spectra were  
101 determined, because gas-phase cells may have potential wall loss problems and thus the  
102 quantitative gas-phase cross sections are difficult to measure. We compared isopropyl nitrate and  
103 MACR with isoprene nitrooxy enal, because MACR has the enal structure, and isopropyl nitrate  
104 has the nitrooxy group, and the combination of these two compounds helps to illustrate the  
105 absorption features of the nitrooxy enal studied in this work. The absorption cross section of the  
106 carbonyl nitrate is enhanced relative to that of MACR, but the two spectra have similar features  
107 from 320 nm to 400 nm with peak absorption at 325 nm. This is probably because they both contain  
108 the O=C-C=C chromophore. Below 320 nm the absorption of the ~~carbonyl nitrate~~nitrooxy enal is  
109 enhanced significantly in comparison with that of isopropyl nitrate. This observation is consistent  
110 with reports from Müller et al. (2014) that molecules containing  $\alpha,\beta$ -nitrooxy ketone functionalities  
111 have enhanced UV absorption.

## 112 3 Methods

### 113 3.1 Setup for the kinetics chamber experiments

114 Three sets of reaction chamber experiments were conducted to determine the photolysis frequency,  
115 OH oxidation rate constant and the O<sub>3</sub> oxidation rate constant for the ~~carbonyl nitrate~~isoprene

Formatted: Font color: Auto

116 nitrooxy enal. Since this work is focused on the photochemistry of the nitrooxy enal, which  
117 describes the loss-dominant processes after sunrise, we did not include experiments concerning  
118 the NO<sub>3</sub>-initiated oxidation processes for this compound. The experiments were performed in the  
119 5500 L Purdue photochemical reaction chamber (Chen et al., 1998). A chemical ionization mass  
120 spectrometer (CIMS) with I<sup>-</sup> as the reagent ion (Xiong et al., 2015) was used to quantify the  
121 ~~earbonyl nitrate~~nitrooxy enal (observed at nominal mass m/z 272) and its nitrate degradation  
122 products (~~Xiong et al., 2015~~). The CIMS has unit mass resolution. Since pure isoprene nitrooxy  
123 enal was introduced into the reaction as the precursor, we do not expect significant interference  
124 from the isotope signal of m/z 271. The chamber air was sampled into the CIMS through a 5.2 m  
125 long FEP tubing (0.8 cm ID, heated to constant 50 °C). The residence time for the sampling tubing  
126 was approximately 5 s, and laminar flow was maintained. To assess the influence of the heated  
127 inlet on the stability of the nitrooxy enal, we have sampled the nitrooxy enal using the heated 50 °C  
128 inlet and using a 20 cm room temperature inlet, and there was no significant difference in their  
129 corresponding CIMS signals. In addition, the *trans*-isoprene nitrooxy enal was synthesized in an  
130 oil bath maintained at 70 °C, but the formation of the *cis* isomer was not observed. Therefore, we  
131 do not consider that there is significant thermal isomerization inside our sampling line. The  
132 photolysis frequency was obtained by measuring the loss of the ~~earbonyl nitrate~~nitrooxy enal  
133 inside the reaction chamber in the presence of UV radiation and propene as a radical scavenger.  
134 When the UV lamps were turned off, the wall loss rate constant for the ~~earbonyl nitrate~~nitrooxy  
135 enal was ~~derived~~derived by observing its slow decay, with propene as an ozone and NO<sub>3</sub>  
136 scavenger. The OH reaction rate constant and O<sub>3</sub> reaction rate constant were obtained using the  
137 relative rate method (Atkinson and Aschmann, 1985). Propene was used as the reference  
138 compound, and its changing concentrations were measured using a GC-FID equipped with a 0.32  
139 mm Rtx-Q-Bond column. For the OH oxidation experiments, OH was generated through the  
140 photolysis of isopropyl nitrite, which was synthesized following Noyes (1933). NO was added  
141 to the chamber to suppress the formation of O<sub>3</sub>. In addition, two OH oxidation experiments were  
142 performed without propene in order to quantify the oxidation products. For the OH-initiated  
143 oxidation experiments, NO and NO<sub>2</sub> were measured using the Total REactive Nitrogen Instrument  
144 (TRENI) (Lockwood et al., 2010). The ozonolysis experiments were performed in the dark, and  
145 cyclohexane was added to the chamber as an OH scavenger. The initial conditions for the  
146 experiments are listed in Table S1.

Formatted: Font color: Auto

Formatted: Font color: Auto

Formatted: Font color: Auto

Formatted: Font: Italic, Font color: Auto

Formatted: Font color: Auto

Formatted: Font: Italic

Formatted: Font color: Auto

## 147 3.2 Computational methods

148 The theoretical UV absorption spectra of the ~~carbonyl nitrate~~isoprene nitrooxy enal, MACR,  
149 isopropyl nitrate and *n*-butyl nitrate in the gas phase were calculated separately and analyzed, in  
150 four stages, using time-dependent density functional theory (TDDFT; (Hohenberg and Kohn, 1964;  
151 Kohn and Sham, 1965; Runge and Gross, 1984)). All calculations were carried out using the  
152 computational chemistry package Q-Chem 4.3 (Shao et al., 2015). First, the structure of each  
153 molecule was optimized employing the long-range corrected hybrid density functional  $\omega$ B97X-D  
154 (Chai and Head-Gordon, 2008) with the 6-31+G\* basis set (Frisch et al., 1984). A high accuracy  
155 grid was employed. Second, frequency ies calculations were executed on the optimized structures  
156 to verify their accuracy. These were run using the same setup described above. Third, after assuring  
157 the structures represented adequate minima, the first ten singlet excited states of each molecule  
158 were computed with TDDFT, using the same functional and basis set. Finally, a visual analysis of  
159 the molecular orbitals (MOs) was carried out with the visualization software IQmol 2.7 (Gilbert,  
160 2012).

## 161 4 Results

### 162 4.1 Absorption spectra and density functional calculations

163 Fig. 4 shows the TDDFT UV absorption spectra of the ~~carbonyl nitrate~~nitrooxy enal, MACR,  
164 isopropyl nitrate and *n*-butyl nitrate. There are three groups of transitions in the simulated spectra.  
165 Unlike the absorption bands depicted in Fig 3, the theoretical gas-phase spectra in Fig. 4 are  
166 showing only the electronic transition lines. To accurately capture the broadening of these lines in  
167 TDDFT so as to simulate absorption bands, we have to consider the effect of the chromophore's  
168 vibrational degrees of freedom and/or to include a condensed phase environment that surrounds  
169 the chromophore. However, explicit modeling of broadening either due to vibronic interactions or  
170 solvent effects is computationally challenging and beyond the scope of this work.

171  
172 Both MACR and the ~~carbonyl nitrate~~nitrooxy enal show a relatively weak transition in the region  
173 around 330 nm, which corresponds to the first electronic transition, from the highest occupied  
174 molecular orbital (HOMO) to the lowest unoccupied molecular orbital (LUMO), in both molecules.

Formatted: Font color: Auto

175 Fig. 5a provides comparative information between the first electronic transition of the ~~carbonyl~~  
176 ~~nitrate~~nitrooxy enal and the homologous excitation of MACR. As shown in Fig. 5a the character  
177 of the molecular orbitals involved in this transition is similar in both cases, indicating that the  
178 aldehyde group is involved in the first electronic excitation of the ~~carbonyl nitrate~~nitrooxy enal.

179 Fig. 5b shows the information corresponding to the second electronic transition of the ~~carbonyl~~  
180 ~~nitrate~~nitrooxy enal and ~~its~~the homologous excitation ~~in~~of isopropyl nitrate and *n*-butyl nitrate.  
181 ~~Both~~ These three transitions are found in the region around 255 nm. The second electronic  
182 transition of the nitrooxy enal is 3 orders of magnitude weaker than its first excitation, located at  
183 330 nm, and they are 3 orders of magnitude darker than those at 330 nm. Inspection of the  
184 character of the MOs involved in these processes reveals a correspondence between the second  
185 electronic excitation of the ~~carbonyl nitrate~~nitrooxy enal, HOMO-2 → LUMO+1, and the HOMO  
186 → LUMO transitions in both isopropyl nitrate and *n*-butyl nitrate. As with the previous case,  
187 that observation confirms that the nitrate group is involved in the second electronic excitation of  
188 the ~~carbonyl nitrate~~nitrooxy enal, ~~but at wavelengths shorter than present at the Earth's surface.~~

189 Fig. 5b also shows that in this case, the local character of the MOs involved in the transition is  
190 even more pronounced, with bulky lobes placed mainly over the nitrate group.

191 Even though the second electronic transition of carbonyl nitrate is not displayed in the  
192 experimental spectra of Fig. 3, because its range covers from 280 nm to 410 nm, it is reasonable  
193 to assume that it is caused by the local excitation of the nitrate group, based on the computational  
194 results. Thus, it can be suggested that the experimental UV absorption spectrum~~um~~a of isopropyl  
195 nitrate is comparable to ~~those that~~ of isopropyl nitrate and *n*-butyl nitrate simulated computationally.  
196 Thus it is possible that the feature in the region around 280 nm of the ~~carbonyl nitrate~~nitrooxy enal  
197 experimental spectrum ~~in~~ef Fig. 3 could be caused by a broadening of the transition located around  
198 255 nm.

199 Another plausible explanation of the feature around 280 nm for the nitrooxy enal would be a  
200 broadening of its brightest transition in the modeled spectrum. It is located around 210 nm, and it  
201 is 3 orders of magnitude brighter than the one at 330 nm. In that region,

202 The brightest transition in the modeled spectra of the carbonyl nitrate, 3 orders of magnitude  
203 brighter than the ones at 330 nm, is located around 210 nm. There are two transitions in this region



204 and each one has a homologous excitation: the HOMO-1 → LUMO in carbonyl nitrate nitrooxy  
205 enal is similar to HOMO-1 → LUMO in MACR, and the HOMO-5 → LUMO+1 in carbonyl  
206 nitrate nitrooxy enal is related to the (mainly) HOMO-1 → LUMO transitions of isopropyl nitrate  
207 and n-butyl nitrate. These transitions are beyond the range of the experimental spectra on Fig. 3  
208 and beyond the atmospherically relevant absorption wavelengths. The theoretical calculations  
209 suggest that the nitrooxy group has electronic transitions at 210 nm and 255 nm, but both  
210 wavelengths are outside the solar radiation spectrum near ground. Therefore, we speculate that the  
211 isoprene nitrooxy enal absorbs photons primarily through the first electronic transition concerning  
212 the enal chromophore, instead of the nitrooxy functionality, and the dissociation of the O-NO<sub>2</sub>  
213 bond (Sect. 4.3.2) likely results from intramolecular energy redistribution.

Formatted: Font color: Auto

#### 214 4.2 Photochemical sinks of 4,1-carbonyl nitrate the 4,1-isoprene nitrooxy enal

215 Fig. 6 shows the first-order wall loss and photolysis loss of the carbonyl nitrate nitrooxy enal inside  
216 the reaction chamber. The wall loss rate constant was  $1.3(\pm 0.42) \times 10^{-5} \text{ s}^{-1}$  (95% confidence  
217 interval), and the photolysis rate constant was  $3.0(\pm 0.42) \times 10^{-5} \text{ s}^{-1}$  (95%), after subtracting the wall  
218 loss rate constant from the first-order decay rate constant measured for the photolysis experiments.

219 The radiation intensity inside the chamber is approximately 10% of solar radiation. Therefore, our  
220 photolysis rate constant is small, making the wall loss rate constant significant, compared with the  
221 photolysis frequency. It is worth mentioning that our reactant carbonyl nitrate nitrooxy enal has a

Formatted: Font color: Auto

222 *trans* configuration, and it may photo-isomerize into the *cis* configuration, which would be  
223 detected at the same *m/z* by the CIMS. The *cis*-carbonyl nitrate nitrooxy enal can either photo-

Formatted: Font: Italic

224 dissociate or isomerize to re-form the *trans* isomer. Our previous work suggests that the CIMS is  
225 4 times more sensitive to the *cis* configuration than the *trans* configuration (Xiong et al., 2015). If  
226 a significant amount of the *cis* isomer was present, the CIMS signal should resemble a double  
227 exponential curve. If the lifetime for the *trans* → *cis* reaction is comparable to the duration of the  
228 experiments (approximately 3 hours), we would expect the CIMS signal to resemble a double  
229 exponential curve, because the *cis* isomer was being produced and consumed simultaneously. This

Formatted: Font: Italic

Formatted: Font: Italic

230 double exponential curve is not observed for the photolysis data (Fig. 6). If a *cis-trans* equilibrium  
231 is established instantaneously, the CIMS signal would still be a single exponential curve, which  
232 represent the loss of both isomers. However, given the similar nitrooxy enal structures for the *cis*  
233 and *trans* isomers, we do not expect their photolysis frequencies to differ significantly, so the total

Formatted: Font: Italic

Formatted: Font: Italic

234 photolysis rate constant obtained from the CIMS measurement can be used as the photolysis  
235 frequency for the individual *cis* or *trans* isomer. ~~In an extreme scenario with rapid *trans* → *cis*~~  
236 ~~isomerization, the CIMS signal should increase under radiation, due to the higher sensitivity of the~~  
237 ~~*cis* isomer. For our carbonyl nitrate photolysis experiments, a single exponential decay in the~~  
238 ~~CIMS signal was observed, indicating insignificant contribution from the *cis* isomer. Hence,~~  
239 ~~Therefore, regardless of the *trans* → *cis* isomerization rate,~~ our measured photolysis frequency  
240 should well characterize the loss rate of the ~~carbonyl nitrate precursor *trans*-nitrooxy enal~~ inside  
241 the reaction chamber.

Formatted: Font: Italic

Formatted: Font: Italic

Formatted: Font: Italic

242 Since the UV radiation inside the reaction chamber is different from the UV radiation in the  
243 ambient environment (Fig. 7), Cl<sub>2</sub> was used as a reference compound to ~~extrapolate-translate~~  
244 the nitrate photolysis rate from chamber radiation to solar radiation. The photolysis decay of Cl<sub>2</sub> in the  
245 reaction chamber was measured with the CIMS (Neuman et al., 2010). Cyclohexane was added to  
246 the chamber to scavenge the Cl atoms so that Cl<sub>2</sub> was not re-formed from Cl + Cl recombination.  
247 The first-order photolysis rate constant for Cl<sub>2</sub> was 2.50(±0.0408)×10<sup>-4</sup> s<sup>-1</sup> (Fig. S4).

248 The photolysis frequency (J) is the integrated product of quantum yield (Φ), absorption cross  
249 section (σ, cm<sup>2</sup>) and actinic flux (F, cm<sup>-2</sup> s<sup>-1</sup>) across all wavelengths (Eq. 1). Therefore, the  
250 photolysis frequencies for the ~~carbonyl nitrate nitrooxy enal~~ and Cl<sub>2</sub> in the reaction chamber can  
251 be compared as in Eq. 2.

$$252 \quad J = \int \Phi_{\lambda} \sigma_{\lambda} F_{\lambda} d\lambda \quad (\text{Eq. 1})$$

$$253 \quad \frac{J_{\text{Cl}_2}^{\text{chamber}}}{J_{\text{nitrate}}^{\text{chamber}}} = \frac{\sum \Phi_{\text{Cl}_2} \sigma_{\text{Cl}_2} F_{\text{chamber}}}{\sum \Phi_{\text{nitrate}} \sigma_{\text{nitrate}} F_{\text{chamber}}} \quad (\text{Eq. 2})$$

254  $J_{\text{Cl}_2}^{\text{chamber}}$  and  $J_{\text{nitrate}}^{\text{chamber}}$  are the photolysis frequencies of Cl<sub>2</sub> and the ~~carbonyl nitrate nitrooxy enal~~  
255 inside the chamber.  $\sigma_{\text{Cl}_2}$  and  $\sigma_{\text{nitrate}}$  are the cross sections for Cl<sub>2</sub> and the ~~carbonyl nitrate nitrooxy~~  
256 ~~enal~~ at each wavelength.  $\sigma_{\text{nitrate}}$  was determined by this work (Fig. 3).  $\sigma_{\text{Cl}_2}$  has been measured  
257 previously and the IUPAC recommended values were used (Atkinson et al., 2007).  $F_{\text{chamber}}$  is the  
258 wavelength-dependent flux of photons inside the chamber. The radiation spectrum (Fig. 7) of the  
259 chamber UV lamps (UVA 340) was obtained from the manufacturer (Q-lab), but the actual  
260 absolute radiation intensity in the chamber is expected to differ from the manufacturer's radiation

261 spectrum by a scaling factor, because of the inverse-square dependence on distance, and our  
 262 specific multi-lamp geometry. When Cl<sub>2</sub> was used as a reference compound for the nitrate  
 263 photolysis rate, the scaling factors in Eq. 2 will cancel.

264 The Cl-Cl bond dissociation energy is 243 kJ/mol (Luo, 2007b), equivalent to a photon at 492 nm.  
 265 Since Cl<sub>2</sub> has only one bond, it has unity quantum yield below 492 nm and zero quantum yield  
 266 above 492 nm. The emission spectrum of the UV lamps for the reaction chamber is centered from  
 267 300 nm to 400 nm (Fig. 7). Hence,  $\varphi_{Cl_2} = 1$  in Eq. 2, at all wavelengths. For the ~~carbonyl~~  
 268 ~~nitrate~~~~nitrooxy enal~~, however, its quantum yield is affected by the bond dissociation energy,  
 269 intramolecular vibrational energy redistribution and relaxation of the excited molecule from  
 270 collisions, so an average effective quantum yield ( $\varphi_{nitrate}^{eff}$ ) is assumed, and Eq. 2 becomes Eq. 3.  
 271 Since the photolysis rates, absorption cross sections and chamber radiation spectrum ~~were~~are  
 272 known, we calculated that  $\varphi_{nitrate}^{eff}$  was 0.48.

$$273 \frac{j_{Cl_2}^{chamber}}{j_{nitrate}^{chamber}} = \frac{\sum \sigma_{Cl_2} F_{chamber}}{\varphi_{nitrate}^{eff} \sum \sigma_{nitrate} F_{chamber}} \quad (\text{Eq. 3})$$

274 The effective quantum yield of 0.48 indicates that when the ~~carbonyl nitrate~~~~nitrooxy enal~~s absorbs  
 275 a photon inside the reaction chamber, the probability (averaged across the absorption wavelengths)  
 276 for it to dissociate is 48%. However, the probability for nitrate photolysis is not equal at all  
 277 wavelengths, the low energy photons (long wavelength) being less likely to induce photo-  
 278 dissociation. Hence, we introduced a threshold wavelength  $\lambda_0$ , for which the ~~carbonyl~~  
 279 ~~nitrate~~~~nitrooxy enal~~ has unity quantum yield below  $\lambda_0$  and zero quantum yield above  $\lambda_0$ . Although  
 280 this approach accounts for the energy difference of photons with different wavelengths, it is still a  
 281 very rough estimation. Using the threshold wavelength, the effective quantum yield can be  
 282 expressed by Eq. 4 and Eq. 5, where  $\varphi(\lambda)$  is the quantum yield of the ~~carbonyl nitrate~~~~nitrooxy enal~~,  
 283 and  $F(\lambda)$  is the chamber photon flux (Fig. 7), as a function of the wavelength  $\lambda$ . Solving for the  
 284 unknown  $\lambda_0$  in Eq. 5, we calculated that  $\lambda_0$  ~~was~~should be 347 nm.

$$285 \varphi(\lambda) = \begin{cases} 1 & (\lambda \leq \lambda_0) \\ 0 & (\lambda > \lambda_0) \end{cases} \quad (\text{Eq. 4})$$

$$286 \frac{\sum_{\lambda} F(\lambda) \cdot \varphi(\lambda)}{\sum_{\lambda} F(\lambda)} = 0.48 \quad (\text{Eq. 5})$$

287 The solar radiation spectrum was calculated with the TUV model (Madronich and Flocke, 1998).  
288 By assuming that the carbonyl nitrate nitrooxy enal has zero quantum yield above 347 nm and unity  
289 quantum yield below 347 nm, its photolysis frequency is  $2.6 \times 10^{-4} \text{ s}^{-1}$  for a solar zenith angle  
290 (SZA) of  $45^\circ$ , and  $3.7 \times 10^{-4} \text{ s}^{-1}$  for SZA of  $0^\circ$ . It is worth mentioning that the condensed-phase and  
291 gas-phase absorption spectra should be different, because the solvent molecules affect the  
292 polarization and dipole moment of the solute (Bayliss and McRae, 1954; Braun et al., 1991; Linder  
293 and Abdunur, 1971). Although we were unable to measure the gas-phase cross section of the  
294 carbonyl nitrate nitrooxy enal, we could assess the uncertainty caused by using the condensed-  
295 phase spectrum in our calculation, by comparing the gas-phase and condensed-phase spectra of  
296 MACR and isopropyl nitrate (Fig. S5a). On average, the gas-phase absorption cross sections of  
297 MACR and isopropyl nitrate are 1.7 times those in the solution phase (Fig. S5b), calculated as the  
298 ratio of the gas-phase cross sections divided by the condensed-phase cross sections at each  
299 wavelength. For the carbonyl nitrate nitrooxy enal, if the gas-phase cross section is assumed to be  
300 1.7 times that of the solution-phase cross section, the calculated effective quantum yield becomes  
301 0.28, leading to a threshold wavelength ( $\lambda_0$ ) of 336 nm. Using this set of cross section and quantum  
302 yields, we calculated that the nitrate photolysis frequency was  $3.1 \times 10^{-4} \text{ s}^{-1}$  for SZA of  $45^\circ$ , and  
303  $4.6 \times 10^{-4} \text{ s}^{-1}$  for SZA of  $0^\circ$ , which are 19% and 24% larger than results obtained using the  
304 condensed-phase cross section. The calculated ambient photolysis frequency is not affected as  
305 significantly by the change in the absorption cross section, because it is constrained by the  
306 measured photolysis frequency in the reaction chamber. When a larger cross section is applied, a  
307 smaller quantum yield is derived, and the calculated ambient photolysis frequency, being the  
308 integrated product of the cross section, quantum yield and radiation, will not increase as much as  
309 the cross section. In addition to the cross section, our treatment of the wavelength-dependent  
310 quantum yield can also introduce uncertainty to the calculated results. If a constant effective  
311 quantum yield is used in the calculation, the ambient photolysis frequency is  $2.0 \times 10^{-4} \text{ s}^{-1}$  for SZA  
312 of  $45^\circ$ , and  $2.8 \times 10^{-4} \text{ s}^{-1}$  for SZA of  $0^\circ$ , which are 23% and 24% lower than assuming a threshold  
313 wavelength. Therefore, our calculated ambient photolysis frequency, based on condensed-phase  
314 absorption cross section and a threshold energy for unity quantum yield, has an uncertainty of  
315 25%. Since we believe that the cross sections are indeed larger in the gas phase, our best estimate  
316 is  $3.1(\pm 0.8) \times 10^{-4} \text{ s}^{-1}$  for SZA= $45^\circ$ .

Formatted: Font color: Auto

317 Fig. 8 shows the results for the relative rate experiments for the OH-initiated and O<sub>3</sub>-initiated  
318 oxidation of the ~~carbonyl nitrate nitrooxy enal~~, with propene as the reference compound. The loss  
319 of the ~~carbonyl nitrate nitrooxy enal~~ to wall uptake and photolysis is corrected when comparing the  
320 oxidative loss of the nitrate to that of propene, using the same method as Hallquist et al. (1997).  
321 The OH and O<sub>3</sub> oxidation rate constants for propene are  $3.0(\pm 0.5) \times 10^{-11} \text{ cm}^3 \text{ molecules}^{-1} \text{ s}^{-1}$  (Klein  
322 et al., 1984; Zellner and Lorenz, 1984) and  $1.00(\pm 0.06) \times 10^{-17} \text{ cm}^3 \text{ molecules}^{-1} \text{ s}^{-1}$  (Herron and  
323 Huie, 1974; Treacy et al., 1992). These are the IUPAC preferred rate constants for T=298K  
324 (<http://iupac.pole-ether.fr/>). Hence, the OH and O<sub>3</sub> oxidation rate constants for the isoprene  
325 ~~carbonyl nitrate nitrooxy enal~~ are, based on the results from the relative rate experiments,  
326  $4.1(\pm 0.7) \times 10^{-11} \text{ cm}^3 \text{ molecules}^{-1} \text{ s}^{-1}$  and  $4.4(\pm 0.3) \times 10^{-18} \text{ cm}^3 \text{ molecules}^{-1} \text{ s}^{-1}$  respectively, at 295  
327 K.

328 The OH oxidation rate constant for the ~~carbonyl nitrate nitrooxy enal~~ can be estimated through the  
329 structure-activity-relationship (SAR) approach proposed by Kwok and Atkinson (1995). The rate  
330 constant for OH addition to the double bond can be calculated as  $k(-\text{CH}=\text{CH})$ , which is  $8.69 \times 10^{-11}$   
331  $\text{ cm}^3 \text{ molecules}^{-1} \text{ s}^{-1}$ , multiplied by the two correction factors C(-CHO) and C(-CH<sub>2</sub>ONO<sub>2</sub>), which  
332 are 0.34 and 0.47 respectively. The resulting OH addition rate constant is  $1.39 \times 10^{-11} \text{ cm}^3$   
333  $\text{ molecules}^{-1} \text{ s}^{-1}$ . The rate constant for H abstraction from the -CHO group is  $1.61 \times 10^{-11} \text{ cm}^3$   
334  $\text{ molecules}^{-1} \text{ s}^{-1}$ , after multiplying by a correction factor of 1 for having a double bond at its  $\alpha$   
335 position. The rate constant for H abstraction from the methylene group is  $3.7 \times 10^{-14} \text{ cm}^3$   
336  $\text{ molecules}^{-1} \text{ s}^{-1}$ , calculated by multiplying the base rate constant for methylene groups, which is  
337  $9.34 \times 10^{-13} \text{ cm}^3 \text{ molecules}^{-1} \text{ s}^{-1}$ , by the correction factors of the nitrate group and the double bond,  
338 which are 0.04 and 1, respectively. OH addition to the nitrate group has a rate constant of  $4.4 \times 10^{-13}$   
339  $\text{ cm}^3 \text{ molecule}^{-1} \text{ s}^{-1}$ , after taking account of the enhancement factor of 1.23 for the methylene group.  
340 H abstraction from the methyl group has a rate constant of  $1.36 \times 10^{-13} \text{ cm}^3 \text{ molecules}^{-1} \text{ s}^{-1}$ . By  
341 summing up the rate constants for all these reaction pathways, the SAR-derived OH oxidation rate  
342 constant for the ~~4,1-carbonyl nitrate rate constant isoprene nitrooxy enal~~ is  $3.1 \times 10^{-11} \text{ cm}^3$   
343  $\text{ molecules}^{-1} \text{ s}^{-1}$ , approximately 30% lower than the experimental measurement. The dominant  
344 reaction channels are OH addition to the double bond and H abstraction from the aldehyde group.  
345 Contributions from the other reaction pathways are small (<3%).

346 The relative importance of the three photochemical sinks, photolysis, OH oxidation and O<sub>3</sub>  
347 oxidation, depends on the solar radiation and the concentrations of OH and O<sub>3</sub>. To better illustrate  
348 their relative contributions, observations of OH and O<sub>3</sub> from previous field campaigns were used  
349 to calculate the loss rates of the ~~carbonyl nitrate~~nitrooxy enal. The local solar radiation was  
350 calculated with the TUV model (Madronich and Flocke, 1998), which was then used to derive the  
351 photolysis frequency. The calculated results (Fig. 9) suggest that photolysis is a significant  
352 degradation pathway for the ~~carbonyl nitrate~~nitrooxy enal, which can dominate over OH oxidation  
353 toward mid-day. When the solar radiation intensity is small (such as 6:00 AM for the 1999 SOS  
354 campaign), OH oxidation is likely the dominant sink. Due to the fast photolysis and high reactivity  
355 toward OH, the photochemical lifetime of the ~~carbonyl nitrate~~nitrooxy enal can be as short as less  
356 than one hour.

### 357 **4.3 Degradation products of the ~~4,1-carbonyl nitrate~~4,1-isoprene nitrooxy enal**

#### 358 **4.3.1 OH oxidation**

359 The products from the OH-initiated oxidation of the ~~4,1-carbonyl nitrate~~isoprene nitrooxy enal  
360 were observed by the CIMS. The change in the CIMS signals before and after the reaction are  
361 illustrated in Fig. 10, along with assignment of some of the molecular structures based on the  
362 molecular weight and likely chemistry. The OH-initiated oxidation reaction can proceed through  
363 two channels: H abstraction from the aldehyde group and OH addition to the double bond.

364 For the H abstraction pathway, a peroxyacyl nitrate (PAN) product was observed at m/z 349 (Fig.  
365 10), which can be formed as shown in Fig. 11. The first-order dissociation rate constant for the  
366 PAN compound was determined at room temperature (295 K) using the following method. A 100  
367 L Teflon bag containing the air mixture of approximately 1 ppm isopropyl nitrite and 30 ppb  
368 ~~isoprene nitrooxy enal~~4,1-carbonyl nitrate was irradiated, and the PAN compound was formed  
369 ~~from when the nitrooxy enal reacted with~~ OH and NO<sub>2</sub> (produced through the photolysis of  
370 isopropyl nitrite) ~~reaction with the 4,1-carbonyl nitrate~~. After 5 min reaction time, the bag was  
371 removed from the UV radiation, and NO was injected into the bag to around 4 ppm in concentration.  
372 The bag was then sampled simultaneously by the CIMS, which monitored the decrease in the  
373 signal of the PAN compound, and by the TRENI, which monitored the concentrations of NO and  
374 NO<sub>2</sub>. The PAN dissociation reaction is a reversible process, where the dissociation products,

375 peroxyacyl (PA) radical and NO<sub>2</sub>, can re-combine to form PAN. With the addition of the large  
 376 amount of NO, PA radicals are predominantly consumed by the irreversible PA + NO reaction,  
 377 leading to the decay of the PAN compound. The apparent PAN dissociation rate constant can be  
 378 described by Eq. 6 (Shepson et al., 1992), where k is the first-order loss rate constant measured by  
 379 the CIMS (Fig. S6), k<sub>PAN</sub> is the real PAN dissociation rate constant, [NO] and [NO<sub>2</sub>] are the  
 380 concentrations for NO and NO<sub>2</sub>, and k<sub>NO</sub> and k<sub>NO<sub>2</sub></sub> are the rate constants for PA + NO and PA +  
 381 NO<sub>2</sub> reactions. Since the rate constants k<sub>NO</sub> and k<sub>NO<sub>2</sub></sub> for the ~~nitrooxy enal~~~~carbonyl nitrate~~-derived  
 382 PA radical are unknown, the IUPAC recommended rate constants for the peroxyacetyl radicals  
 383 (CH<sub>3</sub>C(O)O<sub>2</sub>) are used, with k<sub>NO</sub> = 2.0×10<sup>-11</sup> cm<sup>3</sup> molecule<sup>-1</sup> s<sup>-1</sup> and k<sub>NO<sub>2</sub></sub> = 8.9×10<sup>-12</sup> cm<sup>3</sup>  
 384 molecule<sup>-1</sup> s<sup>-1</sup>. The PAN dissociation rate constant, after correcting for the competing PA + NO  
 385 and PA + NO<sub>2</sub> reactions using Eq. 6, is 5.7(±0.8)×10<sup>-4</sup> s<sup>-1</sup>, based on three experimental trials. In  
 386 addition to dissociation, the PAN compound in the 100 L bag could also undergo wall loss. This  
 387 loss rate was estimated by multiplying the wall loss rate of the ~~carbonyl nitrate~~~~nitrooxy enal~~ in the  
 388 5500 L chamber by a factor of 16, which is the square diffusion distance of the chamber relative  
 389 to that of the 100 L bag, assuming the PAN compound and the isoprene carbonyl nitrate have  
 390 similar diffusion and adsorption coefficients. Considering the uncertainty in wall loss rate, the  
 391 PAN dissociation rate constant is 5.7(+0.8/-2.8)×10<sup>-4</sup> s<sup>-1</sup>. Previous studies of the dissociation rate  
 392 constants for peroxyacyl nitrates have reported results ranging from 1.6×10<sup>-4</sup> s<sup>-1</sup> to 6.0×10<sup>-4</sup> s<sup>-1</sup> at  
 393 298 K (Bridier et al., 1991; Grosjean et al., 1994; Kabir et al., 2014; Roberts and Bertman, 1992).  
 394 Our result is consistent with previous work.

$$395 \quad k = k_{PAN} \left( 1 - \frac{1}{1 + \frac{k_{NO}[NO]}{k_{NO_2}[NO_2]}} \right) \quad (\text{Eq. 6})$$

396 Since our OH oxidation experiments were conducted in the presence of high NO concentration, a  
 397 significant fraction of the PA radicals from the H abstraction reaction channel were expected to  
 398 react with NO to form alkoxy radicals. Based on the product observed at m/z 321, a reaction  
 399 scheme (Fig. 11) is proposed, where the alkoxy radical dissociates into CO<sub>2</sub> and an ~~alkyl~~~~alkenyl~~  
 400 radical, which is further oxidized to form a C<sub>4</sub> dinitrate (m/z 321, Fig. 10), along with ethanal  
 401 nitrate (m/z 232, Fig. 10).

402 For the OH addition pathway, OH can add to the C<sub>2</sub> and the C<sub>3</sub> position of the ~~4,1-isoprene~~  
 403 ~~carbonyl nitrate~~~~isoprene nitrooxy enal~~, but the less substituted C<sub>3</sub> position should be preferential

404 (Peeters et al., 2007). For the C2 addition, the expected nitrate products are C5 dinitrate and ethanal  
405 nitrate (Fig. 12a), ~~as~~and their nominal masses were observed at m/z 351 and m/z 232 (Fig. 10).  
406 NO<sub>2</sub> could potentially be released with the concurrent formation of a C4 di-aldehyde (Fig. 12a).  
407 The CIMS signal for this compound at m/z 229 did not increase (Fig. 10), but the CIMS sensitivity  
408 for this compound could be relatively low. For the C3 addition, the expected nitrate products are  
409 C5 dinitrate, MVK nitrate and ethanal nitrate (Fig. 12b), observed at m/z 351, m/z 276 and m/z  
410 232 (Fig. 10). We assigned m/z 276 to solely MVK nitrate, instead of MACR nitrate, because the  
411 precursor nitrooxy enal has a secondary carbon at its C3 position, and the OH oxidation reaction  
412 cannot add a functional group at this position while still maintaining it as a secondary carbon as is  
413 the case for MACR nitrate. The C2 and C3 OH addition pathway would lead to two C5 dinitrate  
414 isomers, but they were detected at the same mass by the CIMS.

415 Using a GC-ECD/CIMS method similar to the one described by Xiong et al. (2015), the CIMS  
416 sensitivities of the nitrate products were determined relative to the CIMS sensitivity of the ~~4,1-~~  
417 ~~carbonyl nitrate~~isoprene nitrooxy enal. The setup was modified to operate the GC separation under  
418 pressure lower than 1 atm (Fig. S7), which helped to lower the elution temperature. A Teflon bag  
419 filled with the ~~4,1-carbonyl nitrate~~nitrooxy enal, isopropyl nitrite, and NO was irradiated to  
420 generate the OH oxidation products. The mixture of the ~~4,1-carbonyl nitrate~~nitrooxy enal and its  
421 products ~~was~~ere then cryo-focused and separated on the GC column, and ~~the~~ eluent species were  
422 detected by the ECD and the CIMS simultaneously. We were able to quantify the MVK nitrate  
423 and the ethanal nitrate using this method, assuming identical ECD sensitivities for nitrates. The  
424 other products shown in Fig. 10, however, were not detected with simultaneous good signal-to-  
425 noise ratio on the ECD and the CIMS. The ECD/CIMS chromatograms are shown in Fig. 13. We  
426 determined that the reaction of the ~~4,1-carbonyl nitrate~~isoprene nitrooxy enal ~~and with~~ the reagent  
427 ion I<sup>-</sup> could form NO<sub>3</sub><sup>-</sup>, but the same reaction did not occur for the MVK nitrate and the ethanal  
428 nitrate (Fig. 13). Formation of NO<sub>3</sub><sup>-</sup> from I<sup>-</sup> reaction with organic nitrates has not been reported  
429 previously. Since I<sup>-</sup> is a poor nucleophile, it is unclear if this reaction proceeds by S<sub>N</sub>2 substitution.  
430 Using the same I<sup>-</sup> ionization method, Wang et al. (2014) observed NO<sub>3</sub><sup>-</sup> signal equivalent to a NO<sub>3</sub>  
431 + N<sub>2</sub>O<sub>5</sub> concentration of 200-1000 ppt during a field study in Hong Kong. Through interference  
432 tests, the authors attributed 30-50% of the observed NO<sub>3</sub><sup>-</sup> signal to the interference from  
433 peroxyacetyl nitrate and NO<sub>2</sub>. Since I<sup>-</sup> reaction with the ~~carbonyl nitrate~~nitrooxy enal can also  
434 generate NO<sub>3</sub><sup>-</sup>, organic nitrates (RONO<sub>2</sub>) could be a potential source of interference for NO<sub>3</sub><sup>-</sup>.

Formatted: Font color: Auto



435 N<sub>2</sub>O<sub>5</sub> measurement with the I<sup>-</sup> ionization method. For field measurement of isoprene nitrooxy enal,  
436 this compound could be mistakenly measured as NO<sub>3</sub><sup>-</sup> when iodide-based CIMS was used without  
437 tuning the instrument specifically to favor iodide-nitrate clustering. While no field observations of  
438 this type of compound have been reported to date, they can still potentially be an important NO<sub>y</sub>  
439 reservoir. For instance, Brown et al. (2009) estimated that in the 2004 NEAQS study the total  
440 concentration of nitrates derived from NO<sub>3</sub> + isoprene chemistry could reach 500 ppt. The carbonyl  
441 nitrates (nitrooxy enone and nitrooxy enal) can contribute to a significant fraction of the total.

442 For the GC-ECD/CIMS calibration, 9 trials were conducted at three different pressures. The results  
443 are summarized in Table S2. The relative CIMS sensitivities for the nitrooxy enal~~4,1-carbonyl~~  
444 ~~nitrate~~, ethanal nitrate and MVK nitrate are 1:15(±3):34(±3) respectively. The absolute CIMS  
445 sensitivity of the ~~4,1-carbonyl nitrate~~isoprene nitrooxy enal was determined with standard gas  
446 samples prepared following Xiong et al. (2015), and the result was used to calculate the absolute  
447 sensitivities for the ethanal nitrate and the MVK nitrate. The ethanal nitrate and the MVK nitrate  
448 both have the -ONO<sub>2</sub> group at the β position of the acidic H, so their CIMS sensitivities are  
449 comparable. For the MVK nitrate, the electron-withdrawing ketone group can further enhance its  
450 gas-phase acidity and its affinity to bind with I<sup>-</sup>. Hence, the CIMS sensitivity for the MVK nitrate  
451 is greater than for the ethanal nitrate. For the ~~4,1-carbonyl nitrate~~nitrooxy enal, its low CIMS  
452 sensitivity can be caused by the *trans*-δ configuration of the -ONO<sub>2</sub> group and the -CHO group.  
453 Our previous studies on isoprene-derived hydroxynitrates suggested that the CIMS sensitivity for  
454 the β isomer is 8 times greater than for the *trans*-δ isomer (Xiong et al., 2015). Lee et al. (2014a)  
455 also reported the β isomer sensitivity being over 16 times greater than the *trans*-δ isomer  
456 sensitivity, using iodide as the reagent ion. Hence, our calibration results, with the sensitivity for  
457 the ethanal nitrate 15 times greater than the sensitivity for the ~~4,1-carbonyl nitrate~~nitrooxy enal, is  
458 consistent with previous work.

459 With the CIMS sensitivities determined, the yield of the MVK nitrate and the ethanal nitrate from  
460 the OH-initiated oxidation of ~~4,1-carbonyl nitrate~~the isoprene nitrooxy enal was obtained by  
461 comparing the formation of the products relative to the loss of the reactant (Fig. 14). The yield of  
462 the ethanal nitrate was corrected for loss to OH oxidation and photolysis, using the method  
463 described by Tuazon et al. (1984). The applied ethanal nitrate + OH rate constant was 3.4×10<sup>-12</sup>  
464 cm<sup>3</sup> molecules<sup>-1</sup> s<sup>-1</sup>, calculated using the structure-reactivity relationship (SAR) proposed by

Formatted: Font color: Auto

Formatted: Font color: Auto

Formatted: Font color: Auto

465 Kwok and Atkinson (1995). The applied photolysis frequency for ethanal nitrate was  $1.69 \times 10^{-5}$   
466  $s^{-1}$ , calculated with the cross section recommended by Muller et al. (2014) and a unity quantum  
467 yield. The photolysis frequency of the isoprene carbonyl nitrate was applied to account for the  
468 photolytic loss of ethanal nitrate inside the chamber, because the  $\beta$  ketone group is known to  
469 enhance the absorption cross section of the nitrate (Müller et al., 2014). The yield of the MVK  
470 nitrate was corrected for loss to photolysis, wall uptake and OH oxidation using the same method  
471 as that for the ethanal nitrate yield. For the MVK nitrate, no OH loss correction was applied,  
472 because MVK nitrate is saturated and is not expected to undergo significant loss to OH. The applied  
473 photolysis frequency for the MVK nitrate was  $4.5 \times 10^{-6} s^{-1}$ , calculated using the absorption cross  
474 section of 3-nitrooxy-2-butanone (Barnes et al., 1993) as a surrogate and unity quantum yield  
475 across all wavelengths (Müller et al., 2014). However, its loss to wall uptake and photolysis loss  
476 was corrected, following the same method as used for the ethanal nitrate. The MVK nitrate loss  
477 rates wall loss rate for wall uptake and photolysis inside the chamber were set the same as  
478 those that for the 4,1-carbonyl nitrate nitrooxy enal, because MVK nitrate is also a ketone nitrate,  
479 which is prone to photolysis loss, and it has a molecular weight close to that of the nitrooxy enal 4,1-  
480 carbonyl nitrate. Based on the Kwok and Atkinson (1995) SAR method, we calculated that the rate  
481 constant for MVK nitrate reaction with OH should be  $1.78 \times 10^{-12} cm^3 molecules^{-1} s^{-1}$ . After the  
482 correction for secondary loss, the apparent yield is 24.523.3% for MVK nitrate and 8.088.0% for  
483 ethanal nitrate. Considering the uncertainties in the sensitivities of MVK nitrate and ethanal nitrate  
484 (Table S2), the MVK nitrate yield is 24.23(±3)%, and the ethanal nitrate yield is 8(±2)%. The  
485 fractional inlet sampling loss for the three nitrates was determined by comparing the CIMS signals  
486 of sampling through the 5.2 m long 50°C tubing and through a 20 cm room temperature tubing.  
487 By correcting for the inlet sampling loss, the MVK nitrate yield is 24.23(±5)%, and the ethanal  
488 nitrate yield is 8(±3)%. For the two OH oxidation experiments, the first-order loss rate of the 4,1-  
489 carbonyl nitrate nitrooxy enal was  $3 \times 10^{-4} s^{-1}$  (Fig. S8). Since the total wall uptake and photolysis  
490 loss rate for 4,1-isoprene carbonyl nitrate nitrooxy enal was  $4.3 \times 10^{-5} s^{-1}$ , approximately 85% of  
491 the 4,1-carbonyl nitrate nitrooxy enal was lost to OH oxidation. After correcting for this factor, the  
492 MVK nitrate yield is 28.27(±5)%, and the ethanal nitrate yield is 9(±3)%. While we were able to  
493 determine the yields of MVK nitrate and ethanal nitrate from the OH oxidation reaction, the exact  
494 branching ratios for reactions described in Fig. 11 and 12 cannot be derived. This is because ethanal  
495 nitrate can be produced in both H abstraction and OH addition pathways (including both the (a)

Formatted: Font color: Auto

Formatted: Font color: Auto

Formatted: Font color: Auto

Formatted: Font color: Auto

Formatted: Font color: Auto

496 and (b) pathways). For MVK nitrate, even though it is produced in pathway (b) only, it has ethanal  
497 nitrate as a byproduct, making it impossible for us to determine the branching ratio for pathway  
498 (b).

#### 499 4.3.2 Photolysis

500 Previous work on acetaldehyde suggests that at 313 nm the dominant photolysis reaction is  
501 dissociation of the C-CHO bond, forming a formyl radical ( $\bullet\text{CHO}$ ) (Blacet and Loeffler, 1942).  
502 At shorter wavelength (265 nm), the reaction can proceed by intramolecular rearrangement  
503 forming  $\text{CH}_4$  and CO (Blacet and Loeffler, 1942). For compounds with longer carbon chain length,  
504 such as propyl- and butyl- aldehydes, the photo-dissociation reaction can produce alkenes and  
505 smaller aldehydes at 238 nm and 187 nm (Blacet and Crane, 1954). Since the UV radiation that  
506 reaches the earth's surface is mostly above 300 nm, the formyl radical pathway is expected to be  
507 the most important photolysis reaction for alkyl aldehydes (Shepson and Heicklen, 1982). For the  
508 isoprene ~~carbonyl nitrate~~nitrooxy enal, the C-CHO bond is strengthened by the delocalized  
509 electrons from the vinyl and the carbonyl groups, leading to a bond dissociation energy of 413  
510 kJ/mol, as measured for acrolein, which is larger than the C-CHO bond dissociation energy of  
511 acetaldehyde (355 kJ/mol) (Wiberg et al., 1992). In comparison, the O-NO<sub>2</sub> bond dissociation  
512 energy is 175 kJ/mol (Luo, 2007a), much lower than the dissociation energy of the C-CHO bond.  
513 Hence, dissociation of the weak O-NO<sub>2</sub> bond may be an important reaction pathway for the  
514 ~~carbonyl nitrate~~nitrooxy enal. This process likely involves the absorption of a photon by the  
515 C=C-C=O chromophore, followed by intramolecular energy redistribution to deposit energy into  
516 the O-NO<sub>2</sub> bond prior to dissociation. This reaction step would generate NO<sub>2</sub> and an alkoxy radical,  
517 which upon reaction with O<sub>2</sub> forms a conjugated dialdehyde.

518 Fig. 15 shows the CIMS spectra before and after the photolysis of the isoprene ~~carbonyl~~  
519 ~~nitrate~~nitrooxy enal. Cyclohexane was used as the OH scavenger for this experiment. The CIMS  
520 signal for the dialdehyde, which is the O-NO<sub>2</sub> bond dissociation product (reaction mechanism  
521 shown in Fig. 16), did not increase significantly. This may be because the CIMS was not sensitive  
522 to the dialdehyde, and/or the dialdehyde underwent rapid secondary reactions, rendering its steady-  
523 state concentration below the CIMS detection limit. Alternatively, it is possible that the alkoxy  
524 radical derived from O-NO<sub>2</sub> bond dissociation undergoes a 1,5-H shift reaction (Fig. 16),  
525 rendering the formation of the dialdehyde an insignificant pathway. The resulting alkyl radical can

526 immediately form a peroxy radical, which may follow the H shift mechanism proposed by Peeters  
527 et al. (2009) and form a hydroperoxy aldehyde (HPALD) compound, as observed at m/z 257 by  
528 the CIMS (Fig. 15). When the peroxy radical reacts with NO or RO<sub>2</sub>, the resulting alkoxy radical  
529 will form a hydroxy dialdehyde (Fig. 16) with m/z ratio at 241, which was also observed by the  
530 CIMS (Fig. 14). It is worth noting that we also observed CIMS signals for the deprotonated ions  
531 derived from the HPALD compound (m/z 129 and m/z 147) and the hydroxy dialdehyde (m/z 113  
532 and m/z 131). The proton transfer reaction between the iodide ion and alcohols/peroxides have not  
533 been observed previously, but it is possible that the conjugated structures help stabilize the charge  
534 and hence make the proton transfer reaction a viable reaction channel.

535 The product at m/z 276 has the molecular weight of MVK nitrate. In the presence of OH scavenger,  
536 however, the reaction is unlikely to proceed by the OH-initiated oxidation pathway to form MVK  
537 nitrate. Instead, we hypothesize that the isoprene ~~carbonyl nitrate~~ nitrooxy enal could dissociate via  
538 the C-CHO bond, which, following reaction with O<sub>2</sub> and HO<sub>2</sub>, would form a vinyl hydroperoxide  
539 with the same molecular weight as MVK nitrate. Vinyl hydroperoxides are known to be a reactive  
540 intermediate from the intramolecular H shift of Criegee biradical, which can decompose into OH  
541 and alkoxy radicals (Kroll et al., 2002). However, the un-energized vinyl hydroperoxides should  
542 have a lifetime long enough to be detected by mass spectrometers (Liu et al., 2015). In fact,  
543 theoretical calculations suggest that at 25 °C vinyl hydroperoxide has a lifetime of 58 hours  
544 (Richardson, 1995). Therefore, the product at m/z 276 is likely the vinyl hydroperoxide. For the  
545 OH oxidation product experiments, however, we attributed m/z 276 to MVK nitrate only, because  
546 RO<sub>2</sub> + NO reaction (forming MVK nitrate) should dominate over RO<sub>2</sub> + HO<sub>2</sub> reaction (forming  
547 vinyl hydroperoxide), in the presence of high NO concentration.

548 Based on the CIMS spectra of the photolysis products, we conclude that the photolysis of the  
549 isoprene ~~carbonyl nitrate~~ nitrooxy enal leads to the dissociation of both the O-NO<sub>2</sub> and the C-CHO  
550 bonds. A reaction scheme is proposed in Fig. 16. While we were able to identify some of the  
551 photolysis products based on the nominal masses observed with the CIMS, the branching ratio for  
552 the two reaction pathways was not determined, due to lack of quantitative measurements during  
553 the photolysis experiment. Future studies are needed to evaluate the relative importance of these  
554 two processes.

## 555 5 Conclusions and future work

556 An isoprene-derived ~~carbonyl-nitrate~~nitrooxy enal model compound was synthesized to study its  
557 photochemical degradation chemistry in the atmosphere. The UV absorption spectrum of this  
558 compound has contributions from both the C=C-C=O and the -ONO<sub>2</sub> chromophores, as is  
559 confirmed by theoretical calculations, but absorption in the actinic region involves a transition  
560 involving the ~~enale~~carbonyl group. The combination of the C=C-C=O and the -ONO<sub>2</sub>  
561 chromophores enhances the UV cross section of this molecule relative to alkyl nitrates, making  
562 photolysis its dominant daytime sink. The photochemical lifetime of the ~~carbonyl-nitrate~~nitrooxy  
563 enal can be less than one hour, due to its rapid photolysis loss, together with high reactivity toward  
564 OH and O<sub>3</sub>. The OH and O<sub>3</sub> oxidation rate constants for the 4,1-isoprene ~~carbonyl-nitrate~~nitrooxy  
565 enal obtained in this study were both smaller than the reported rate constants for the δ-isoprene  
566 hydroxy nitrates (Jacobs et al., 2014; Lee et al., 2014b). This could be because the oxidation by  
567 either OH or O<sub>3</sub> would break the resonance structure of the C=C-C=O moiety, thus increasing the  
568 activation energy.

569 Using the iodide-based CIMS, we identified the first-generation nitrate products from the OH-  
570 initiated oxidation of the synthesized ~~carbonyl-nitrate~~nitrooxy enal, including mononitrate,  
571 dinitrate and nitrooxy peroxyacyl nitrate. Two of the products, the MVK nitrate and the ethanal  
572 nitrate, were quantified, which together contributed to 37.36(±5)% of the total products. The CIMS  
573 spectra of the nitrate photolysis products suggest that both the C-CHO bond and the O-NO<sub>2</sub> bond  
574 dissociate in the reaction. Since photolysis is a significant sink for the ~~carbonyl-nitrate~~nitrooxy  
575 enal, it is important for future studies to investigate the relative importance of the two reaction  
576 pathways, in order to fully understand the fate of NO<sub>x</sub> in isoprene-rich atmospheres. Dissociation  
577 of the O-NO<sub>2</sub> bond may afford highly oxidized alcohol and hydroperoxide, which can potentially  
578 undergo uptake into the particle phase and facilitate the formation of secondary organic aerosols.  
579 The C-CHO dissociation pathway may form a vinyl hydroperoxide product.

580 The NO<sub>3</sub>-initiated isoprene oxidation can produce a series of isomeric carbonyl nitrates. The 1,4-  
581 ~~carbonyl-nitrooxy enal~~nitrate, which is the dominant isomer, is expected to have similar photolysis  
582 reactivity as the 4,1-~~carbonyl-nitrate~~nitrooxy enal studied in this work, because they both have the  
583 O=C-C=C-C chromophore and the -ONO<sub>2</sub> chromophore, which would enhance the molecular

584 absorption cross section. For the unsaturated ketones (enones) derived from isoprene oxidation,  
585 the ketone functionality may reduce their reactivity toward OH, in comparison with aldehydes, but  
586 we expect them to have similar photochemical properties as the nitrooxy enals, since isomers such  
587 as methyl vinyl ketone (MVK) and methacrolein (MACR) have similar absorption cross sections  
588 and quantum yields (Gierczak et al., 1997).

589 ~~The influence of the unsaturated ketone functionality on nitrate photolysis is still unclear, and~~  
590 ~~future studies are needed to understand how the different conjugated structures can affect the~~  
591 ~~photochemical processes.~~

592 The experiments in this work were conducted in the presence of relatively high NO concentration.  
593 In the ambient environment, organic nitrates produced in the high NO<sub>x</sub> regime can undergo  
594 photochemical degradation in the low NO regime, due to the wide span of ambient NO<sub>x</sub>  
595 concentrations (Su et al., 2015; Xiong et al., 2015). Crouse et al. (2012) proposed that under low  
596 NO conditions, the oxidation of methacrolein (MACR) can regenerate OH radicals and form a  
597 lactone that is prone to reactive uptake onto the aerosol phase. Since the ~~4,1-carbonyl~~  
598 ~~nitrate~~ isoprene nitrooxy enal has a structure similar to that of MACR, it might also undergo similar  
599 reaction in the clean environment. Further experimental work is needed to investigate how the  
600 photochemical oxidation process of the ~~carbonyl-nitrate~~ nitrooxy enal can influence the formation  
601 of OH radicals and growth of secondary organic aerosols.

## 602 Acknowledgement

603 This research was supported in part through computational resources provided by Information  
604 Technology at Purdue University. We thank the National Science Foundation for supporting CHB  
605 and LVS (grant CHE-1465154), and FX and PBS (grant AGS-1228496).

## 606 References

607 Aschmann, S. M., Tuazon, E. C., Arey, J., and Atkinson, R.: Products of the OH radical-initiated  
608 reactions of 2-propyl nitrate, 3-methyl-2-butyl nitrate and 3-methyl-2-pentyl nitrate,  
609 Atmospheric Environment, 45, 1695-1701, <http://dx.doi.org/10.1016/j.atmosenv.2010.12.061>,  
610 2011.

611 Atkinson, R., and Aschmann, S. M.: Kinetics of the gas phase reaction of Cl atoms with a series of  
612 organics at  $296 \pm 2$  K and atmospheric pressure, *International Journal of Chemical Kinetics*, 17,  
613 33-41, 10.1002/kin.550170105, 1985.

614 Atkinson, R., Baulch, D. L., Cox, R. A., Crowley, J. N., Hampson, R. F., Hynes, R. G., Jenkin, M. E.,  
615 Rossi, M. J., and Troe, J.: Evaluated kinetic and photochemical data for atmospheric chemistry:  
616 Volume III &ndash; gas phase reactions of inorganic halogens, *Atmos. Chem. Phys.*, 7, 981-1191,  
617 10.5194/acp-7-981-2007, 2007.

618 Barnes, I., Becker, K. H., and Zhu, T.: Near UV absorption spectra and photolysis products of  
619 difunctional organic nitrates: Possible importance as NO<sub>x</sub> reservoirs, *Journal of Atmospheric*  
620 *Chemistry*, 17, 353-373, 10.1007/bf00696854, 1993.

621 Bayliss, N. S., and McRae, E. G.: Solvent Effects in the Spectra of Acetone, Crotonaldehyde,  
622 Nitromethane and Nitrobenzene, *The Journal of Physical Chemistry*, 58, 1006-1011,  
623 10.1021/j150521a018, 1954.

624 Blacet, F. E., and Loeffler, D. E.: The Photolysis of the Aliphatic Aldehydes. XI. Acetaldehyde and  
625 Iodine Mixtures, *Journal of the American Chemical Society*, 64, 893-896, 10.1021/ja01256a045,  
626 1942.

627 Blacet, F. E.: Photochemistry in the Lower Atmosphere, *Industrial & Engineering Chemistry*, 44,  
628 1339-1342, 10.1021/ie50510a044, 1952.

629 Blacet, F. E., and Crane, R. A.: The Photolysis of the Aliphatic Aldehydes. XVII. Propionaldehyde,  
630 n-Butyraldehyde and Isobutyraldehyde at 2380 and 1870 Å, *Journal of the American Chemical*  
631 *Society*, 76, 5337-5340, 10.1021/ja01650a020, 1954.

632 Braun, W., Fahr, A., Klein, R., Kurylo, M. J., and Huie, R. E.: UV gas and liquid phase absorption  
633 cross section measurements of hydrochlorofluorocarbons HCFC-225ca and HCFC-225cb, *Journal*  
634 *of Geophysical Research: Atmospheres*, 96, 13009-13015, 10.1029/91JD01026, 1991.

635 Bridier, I., Caralp, F., Loirat, H., Lesclaux, R., Veyret, B., Becker, K. H., Reimer, A., and Zabel, F.:  
636 Kinetic and theoretical studies of the reactions acetylperoxy + nitrogen dioxide + M .dbrlw.  
637 acetyl peroxyxynitrate + M between 248 and 393 K and between 30 and 760 torr, *The Journal of*  
638 *Physical Chemistry*, 95, 3594-3600, 10.1021/j100162a031, 1991.

639 Brown, S. S., deGouw, J. A., Warneke, C., Ryerson, T. B., Dubé, W. P., Atlas, E., Weber, R. J., Peltier,  
640 R. E., Neuman, J. A., Roberts, J. M., Swanson, A., Flocke, F., McKeen, S. A., Brioude, J., Sommariva,  
641 R., Trainer, M., Fehsenfeld, F. C., and Ravishankara, A. R.: Nocturnal isoprene oxidation over the  
642 Northeast United States in summer and its impact on reactive nitrogen partitioning and  
643 secondary organic aerosol, *Atmos. Chem. Phys.*, 9, 3027-3042, 10.5194/acp-9-3027-2009, 2009.

644 Chai, J.-D., and Head-Gordon, M.: Long-range corrected hybrid density functionals with damped  
645 atom-atom dispersion corrections, *Physical Chemistry Chemical Physics*, 10, 6615-6620,  
646 10.1039/B810189B, 2008.

647 Chameides, W., and Walker, J. C. G.: A photochemical theory of tropospheric ozone, *Journal of*  
648 *Geophysical Research*, 78, 8751-8760, 10.1029/JC078i036p08751, 1973.

649 Chameides, W., Lindsay, R., Richardson, J., and Kiang, C.: The role of biogenic hydrocarbons in  
650 urban photochemical smog: Atlanta as a case study, *Science*, 241, 1473-1475,  
651 10.1126/science.3420404, 1988.

652 Chameides, W. L., Fehsenfeld, F., Rodgers, M. O., Cardelino, C., Martinez, J., Parrish, D.,  
653 Lonneman, W., Lawson, D. R., Rasmussen, R. A., Zimmerman, P., Greenberg, J., Mliddleton, P.,  
654 and Wang, T.: Ozone precursor relationships in the ambient atmosphere, *Journal of Geophysical*  
655 *Research: Atmospheres*, 97, 6037-6055, 10.1029/91JD03014, 1992.

656 Chen, X., Hulbert, D., and Shepson, P. B.: Measurement of the organic nitrate yield from OH  
657 reaction with isoprene, *Journal of Geophysical Research*, 103, 25563, 10.1029/98jd01483, 1998.

658 Crouse, J. D., Knap, H. C., Ornsø, K. B., Jørgensen, S., Paulot, F., Kjaergaard, H. G., and Wennberg,  
659 P. O.: Atmospheric fate of methacrolein. 1. Peroxy radical isomerization following addition of OH  
660 and O<sub>2</sub>, *The journal of physical chemistry. A*, 116, 5756-5762, 10.1021/jp211560u, 2012.

661 Darer, A. I., Cole-Filipiak, N. C., O'Connor, A. E., and Elrod, M. J.: Formation and stability of  
662 atmospherically relevant isoprene-derived organosulfates and organonitrates, *Environmental*  
663 *science & technology*, 45, 1895-1902, 10.1021/es103797z, 2011.

664 Ferris, A. F., McLean, K. W., Marks, I. G., and Emmons, W. D.: Metathetical Reactions of Silver  
665 Salts in Solution. III. The Synthesis of Nitrate Esters<sup>1</sup>, *Journal of the American Chemical Society*,  
666 75, 4078-4078, 10.1021/ja01112a505, 1953.

667 Frisch, M. J., Pople, J. A., and Binkley, J. S.: Self - consistent molecular orbital methods 25.  
668 Supplementary functions for Gaussian basis sets, *The Journal of Chemical Physics*, 80, 3265-3269,  
669 doi:<http://dx.doi.org/10.1063/1.447079>, 1984.

670 Giacobelli, P., Ford, K., Espada, C., and Shepson, P. B.: Comparison of the measured and simulated  
671 isoprene nitrate distributions above a forest canopy, *Journal of Geophysical Research*, 110,  
672 D01304, 10.1029/2004jd005123, 2005.

673 Gierczak, T., Burkholder, J. B., Talukdar, R. K., Mellouki, A., Barone, S. B., and Ravishankara, A. R.:  
674 Atmospheric fate of methyl vinyl ketone and methacrolein, *Journal of Photochemistry and*  
675 *Photobiology A: Chemistry*, 110, 1-10, [http://dx.doi.org/10.1016/S1010-6030\(97\)00159-7](http://dx.doi.org/10.1016/S1010-6030(97)00159-7), 1997.

676 Gilbert, A. T. B.: IQmol molecular viewer, 2012.

677 Gray, G. M.: Method for the preparation of (E)-4-bromo-2-methylbut-2-en-1-al 4288635, 1981.

678 Grosjean, D., Grosjean, E., and Williams, E. L.: Thermal decomposition of C<sub>3</sub>-substituted  
679 peroxyacyl nitrates, *Res Chem Intermed*, 20, 447-461, 10.1163/156856794X00414, 1994.



680 Grossenbacher, J. W., Barket Jr, D. J., Shepson, P. B., Carroll, M. A., Olszyna, K., and Apel, E.: A  
681 comparison of isoprene nitrate concentrations at two forest-impacted sites, *Journal of*  
682 *Geophysical Research: Atmospheres*, 109, D11311, 10.1029/2003JD003966, 2004.

683 Haagen-Smit, A. J.: Chemistry and Physiology of Los Angeles Smog, *Industrial & Engineering*  
684 *Chemistry*, 44, 1342-1346, 10.1021/ie50510a045, 1952.

685 Hallquist, M., Wängberg, I., and Ljungström, E.: Atmospheric Fate of Carbonyl Oxidation Products  
686 Originating from  $\alpha$ -Pinene and  $\Delta^3$ -Carene: Determination of Rate of Reaction with OH and NO<sub>3</sub>  
687 Radicals, UV Absorption Cross Sections, and Vapor Pressures, *Environmental science &*  
688 *technology*, 31, 3166-3172, 10.1021/es970151a, 1997.

689 Hens, K., Novelli, A., Martinez, M., Auld, J., Axinte, R., Bohn, B., Fischer, H., Keronen, P., Kubistin,  
690 D., Nölscher, A. C., Oswald, R., Paasonen, P., Petäjä, T., Regelin, E., Sander, R., Sinha, V., Sipilä, M.,  
691 Taraborrelli, D., Tatum Ernest, C., Williams, J., Lelieveld, J., and Harder, H.: Observation and  
692 modelling of HO<sub>2</sub> radicals in a boreal forest, *Atmospheric Chemistry and Physics*, 14, 8723-8747,  
693 10.5194/acp-14-8723-2014, 2014.

694 Herron, J. T., and Huie, R. E.: Rate constants for the reactions of ozone with ethene and propene,  
695 from 235.0 to 362.0 deg.K, *The Journal of Physical Chemistry*, 78, 2085-2088,  
696 10.1021/j100614a004, 1974.

697 Hohenberg, P., and Kohn, W.: Inhomogeneous Electron Gas, *Physical Review*, 136, B864-B871,  
698 1964.

699 Horowitz, L. W., Fiore, A. M., Milly, G. P., Cohen, R. C., Perring, A., Wooldridge, P. J., Hess, P. G.,  
700 Emmons, L. K., and Lamarque, J.-F.: Observational constraints on the chemistry of isoprene  
701 nitrates over the eastern United States, *Journal of Geophysical Research*, 112, D12S08,  
702 10.1029/2006jd007747, 2007.

703 Hu, K. S., Darer, A. I., and Elrod, M. J.: Thermodynamics and kinetics of the hydrolysis of  
704 atmospherically relevant organonitrates and organosulfates, *Atmospheric Chemistry and Physics*,  
705 11, 8307-8320, 10.5194/acp-11-8307-2011, 2011.

706 Jacobs, M. I., Burke, W. J., and Elrod, M. J.: Kinetics of the reactions of isoprene-derived  
707 hydroxynitrates: gas phase epoxide formation and solution phase hydrolysis, *Atmospheric*  
708 *Chemistry and Physics*, 14, 8933-8946, 10.5194/acp-14-8933-2014, 2014.

709 Kabir, M., Jagiella, S., and Zabel, F.: Thermal Stability of n-Acyl Peroxynitrates, *International*  
710 *Journal of Chemical Kinetics*, 46, 462-469, 10.1002/kin.20862, 2014.

711 Klein, T., Barnes, I., Becker, K. H., Fink, E. H., and Zabel, F.: Pressure dependence of the rate  
712 constants for the reactions of ethene and propene with hydroxyl radicals at 295 K, *The Journal of*  
713 *Physical Chemistry*, 88, 5020-5025, 10.1021/j150665a046, 1984.

714 Kohn, W., and Sham, L. J.: Self-Consistent Equations Including Exchange and Correlation Effects,  
715 Physical Review, 140, A1133-A1138, 1965.

716 Kroll, J. H., Donahue, N. M., Cee, V. J., Demerjian, K. L., and Anderson, J. G.: Gas-Phase Ozonolysis  
717 of Alkenes: Formation of OH from Anti Carbonyl Oxides, Journal of the American Chemical  
718 Society, 124, 8518-8519, 10.1021/ja0266060, 2002.

719 Kwan, A. J., Chan, A. W. H., Ng, N. L., Kjaergaard, H. G., Seinfeld, J. H., and Wennberg, P. O.: Peroxy  
720 radical chemistry and OH radical production during the NO<sub>3</sub>-initiated oxidation of  
721 isoprene, Atmospheric Chemistry and Physics, 12, 7499-7515, 10.5194/acp-12-7499-2012, 2012.

722 Kwok, E. S. C., and Atkinson, R.: Estimation of hydroxyl radical reaction rate constants for gas-  
723 phase organic compounds using a structure-reactivity relationship: An update, Atmospheric  
724 Environment, 29, 1685-1695, [http://dx.doi.org/10.1016/1352-2310\(95\)00069-B](http://dx.doi.org/10.1016/1352-2310(95)00069-B), 1995.

725 Lee, B. H., Lopez-Hilfiker, F. D., Mohr, C., Kurtén, T., Worsnop, D. R., and Thornton, J. A.: An Iodide-  
726 Adduct High-Resolution Time-of-Flight Chemical-Ionization Mass Spectrometer: Application to  
727 Atmospheric Inorganic and Organic Compounds, Environmental science & technology, 48, 6309-  
728 6317, 10.1021/es500362a, 2014a.

729 Lee, L., Teng, A. P., Wennberg, P. O., Crouse, J. D., and Cohen, R. C.: On rates and mechanisms  
730 of OH and O<sub>3</sub> reactions with isoprene-derived hydroxy nitrates, The journal of physical chemistry.  
731 A, 118, 1622-1637, 10.1021/jp4107603, 2014b.

732 Lefohn, A. S., and Foley, J. K.: Establishing Relevant Ozone Standards to Protect Vegetation and  
733 Human Health: Exposure/Dose-Response Considerations, Air & Waste, 43, 106-112,  
734 10.1080/1073161X.1993.10467111, 1993.

735 Linder, B., and Abdulnur, S.: Solvent Effects on Electronic Spectral Intensities, The Journal of  
736 Chemical Physics, 54, 1807-1814, doi:<http://dx.doi.org/10.1063/1.1675088>, 1971.

737 Lippmann, M.: HEALTH EFFECTS OF OZONE A Critical Review, JAPCA, 39, 672-695,  
738 10.1080/08940630.1989.10466554, 1989.

739 Liu, F., Fang, Y., Kumar, M., Thompson, W. H., and Lester, M. I.: Direct observation of vinyl  
740 hydroperoxide, Physical Chemistry Chemical Physics, 17, 20490-20494, 10.1039/C5CP02917A,  
741 2015.

742 Lockwood, A. L., Shepson, P. B., Fiddler, M. N., and Alaghmand, M.: Isoprene nitrates: preparation,  
743 separation, identification, yields, and atmospheric chemistry, Atmospheric Chemistry and Physics,  
744 10, 6169-6178, 10.5194/acp-10-6169-2010, 2010.

745 Lu, K. D., Rohrer, F., Holland, F., Fuchs, H., Bohn, B., Brauers, T., Chang, C. C., Häseler, R., Hu, M.,  
746 Kita, K., Kondo, Y., Li, X., Lou, S. R., Nehr, S., Shao, M., Zeng, L. M., Wahner, A., Zhang, Y. H., and  
747 Hofzumahaus, A.: Observation and modelling of OH and HO<sub>2</sub> concentrations in the Pearl River

748 Delta 2006: a missing OH source in a VOC rich atmosphere, *Atmos. Chem. Phys.*, 12, 1541-1569,  
749 10.5194/acp-12-1541-2012, 2012.

750 Luo, Y.-R.: BDEs of O-X bonds, in: *Comprehensive Handbook of Chemical Bond Energies*, CRC Press,  
751 351, 2007a.

752 Luo, Y.-R.: BDEs in the halogenated molecules, clusters and complexes, in: *Comprehensive*  
753 *Handbook of Chemical Bond Energies*, CRC Press, 1351-1427, 2007b.

754 Madronich, S., and Flocke, S.: The role of solar radiation in atmospheric chemistry, in: *Handbook*  
755 *of Environmental Chemistry*, edited by: Boule, P., Springer-Verlag, Heidelberg, 1-26, 1998.

756 Mao, J., Paulot, F., Jacob, D. J., Cohen, R. C., Crouse, J. D., Wennberg, P. O., Keller, C. A., Hudman,  
757 R. C., Barkley, M. P., and Horowitz, L. W.: Ozone and organic nitrates over the eastern United  
758 States: Sensitivity to isoprene chemistry, *Journal of Geophysical Research: Atmospheres*, 118,  
759 11,256-211,268, 10.1002/jgrd.50817, 2013.

760 Martinez, M., Harder, H., Kovacs, T. A., Simpas, J. B., Bassis, J., Leshner, R., Brune, W. H., Frost, G.  
761 J., Williams, E. J., Stroud, C. A., Jobson, B. T., Roberts, J. M., Hall, S. R., Shetter, R. E., Wert, B.,  
762 Fried, A., Alicke, B., Stutz, J., Young, V. L., White, A. B., and Zamora, R. J.: OH and HO<sub>2</sub>  
763 concentrations, sources, and loss rates during the Southern Oxidants Study in Nashville,  
764 Tennessee, summer 1999, *Journal of Geophysical Research: Atmospheres*, 108, n/a-n/a,  
765 10.1029/2003JD003551, 2003.

766 Mihelcic, D., Holland, F., Hofzumahaus, A., Hoppe, L., Konrad, S., Müsgen, P., Pätz, H. W., Schäfer,  
767 H. J., Schmitz, T., Volz-Thomas, A., Bächmann, K., Schlomski, S., Platt, U., Geyer, A., Alicke, B., and  
768 Moortgat, G. K.: Peroxy radicals during BERLIOZ at Pabstthum: Measurements, radical budgets  
769 and ozone production, *Journal of Geophysical Research: Atmospheres*, 108, n/a-n/a,  
770 10.1029/2001JD001014, 2003.

771 Müller, J. F., Peeters, J., and Stavrou, T.: Fast photolysis of carbonyl nitrates from isoprene,  
772 *Atmospheric Chemistry and Physics*, 14, 2497-2508, 10.5194/acp-14-2497-2014, 2014.

773 Neuman, J. A., Nowak, J. B., Huey, L. G., Burkholder, J. B., Dibb, J. E., Holloway, J. S., Liao, J., Peischl,  
774 J., Roberts, J. M., Ryerson, T. B., Scheuer, E., Stark, H., Stickel, R. E., Tanner, D. J., and Weinheimer,  
775 A.: Bromine measurements in ozone depleted air over the Arctic Ocean, *Atmos. Chem. Phys.*, 10,  
776 6503-6514, 10.5194/acp-10-6503-2010, 2010.

777 Noyes, W. A.: Explanation of the Formation of Alkyl Nitrites in Dilute Solutions; Butyl and Amyl  
778 Nitrites, *Journal of the American Chemical Society*, 55, 3888-3889, 10.1021/ja01336a503, 1933.

779 Parrish, D. D., Lamarque, J. F., Naik, V., Horowitz, L., Shindell, D. T., Staehelin, J., Derwent, R.,  
780 Cooper, O. R., Tanimoto, H., Volz-Thomas, A., Gilge, S., Scheel, H. E., Steinbacher, M., and Fröhlich,  
781 M.: Long-term changes in lower tropospheric baseline ozone concentrations: Comparing  
782 chemistry-climate models and observations at northern midlatitudes, *Journal of Geophysical*  
783 *Research: Atmospheres*, 119, 5719-5736, 10.1002/2013JD021435, 2014.

784 Patchen, A. K., Pennino, M. J., Kiep, A. C., and Elrod, M. J.: Direct kinetics study of the product-  
785 forming channels of the reaction of isoprene-derived hydroxyperoxy radicals with NO,  
786 International Journal of Chemical Kinetics, 39, 353-361, 10.1002/kin.20248, 2007.

787 Paulot, F., Crouse, J. D., Kjaergaard, H. G., Kroll, J. H., Seinfeld, J. H., and Wennberg, P. O.:  
788 Isoprene photooxidation: new insights into the production of acids and organic nitrates, Atmos.  
789 Chem. Phys., 9, 1479-1501, 10.5194/acp-9-1479-2009, 2009.

790 Paulot, F., Henze, D. K., and Wennberg, P. O.: Impact of the isoprene photochemical cascade on  
791 tropical ozone, Atmospheric Chemistry and Physics, 12, 1307-1325, 10.5194/acp-12-1307-2012,  
792 2012.

793 Peeters, J., Boullart, W., Pultau, V., Vandenberg, S., and Vereecken, L.: Structure-Activity  
794 Relationship for the Addition of OH to (Poly)alkenes: Site-Specific and Total Rate Constants, The  
795 Journal of Physical Chemistry A, 111, 1618-1631, 10.1021/jp066973o, 2007.

796 Peeters, J., Nguyen, T. L., and Vereecken, L.: HOx radical regeneration in the oxidation of isoprene,  
797 Physical chemistry chemical physics : PCCP, 11, 5935-5939, 10.1039/b908511d, 2009.

798 Perring, A. E., Wisthaler, A., Graus, M., Wooldridge, P. J., Lockwood, A. L., Mielke, L. H., Shepson,  
799 P. B., Hansel, A., and Cohen, R. C.: A product study of the isoprene+NO<sub>3</sub> reaction, Atmos. Chem.  
800 Phys., 9, 4945-4956, 10.5194/acp-9-4945-2009, 2009.

801 Platt, U., Alicke, B., Dubois, R., Geyer, A., Hofzumahaus, A., Holland, F., Martinez, M., Mihelcic,  
802 D., Klüpfel, T., Lohrmann, B., Pätz, W., Perner, D., Rohrer, F., Schäfer, J., and Stutz, J.: Free Radicals  
803 and Fast Photochemistry during BERLIOZ, Journal of Atmospheric Chemistry, 42, 359-394,  
804 10.1023/A:1015707531660, 2002.

805 Richardson, W. H.: An Evaluation of Vinyl Hydroperoxide as an Isolable Molecule, The Journal of  
806 Organic Chemistry, 60, 4090-4095, 10.1021/jo00118a027, 1995.

807 Rindelaub, J. D., McAvey, K. M., and Shepson, P. B.: The photochemical production of organic  
808 nitrates from  $\alpha$ -pinene and loss via acid-dependent particle phase hydrolysis, Atmospheric  
809 Environment, 100, 193-201, <http://dx.doi.org/10.1016/j.atmosenv.2014.11.010>, 2015.

810 Roberts, J. M.: The atmospheric chemistry of organic nitrates, Atmospheric Environment. Part A.  
811 General Topics, 24, 243-287, [http://dx.doi.org/10.1016/0960-1686\(90\)90108-Y](http://dx.doi.org/10.1016/0960-1686(90)90108-Y), 1990.

812 Roberts, J. M., and Bertman, S. B.: The thermal decomposition of peroxyacetic nitric anhydride  
813 (PAN) and peroxyacetic nitric anhydride (MPAN), International Journal of Chemical Kinetics,  
814 24, 297-307, 10.1002/kin.550240307, 1992.

815 Roberts, J. M., Flocke, F., Stroud, C. A., Hereid, D., Williams, E., Fehsenfeld, F., Brune, W., Martinez,  
816 M., and Harder, H.: Ground-based measurements of peroxy-carboxylic nitric anhydrides (PANs)  
817 during the 1999 Southern Oxidants Study Nashville Intensive, Journal of Geophysical Research:  
818 Atmospheres, 107, ACH 1-1-ACH 1-10, 10.1029/2001JD000947, 2002.

819 Rollins, A. W., Kiendler-Scharr, A., Fry, J. L., Brauers, T., Brown, S. S., Dorn, H. P., Dubé, W. P.,  
820 Fuchs, H., Mensah, A., Mentel, T. F., Rohrer, F., Tillmann, R., Wegener, R., Wooldridge, P. J., and  
821 Cohen, R. C.: Isoprene oxidation by nitrate radical: alkyl nitrate and secondary organic aerosol  
822 yields, *Atmos. Chem. Phys.*, 9, 6685-6703, 10.5194/acp-9-6685-2009, 2009.

823 Runge, E., and Gross, E. K. U.: Density-Functional Theory for Time-Dependent Systems, *Physical*  
824 *Review Letters*, 52, 997-1000, 1984.

825 Schwantes, R. H., Teng, A. P., Nguyen, T. B., Coggon, M. M., Crouse, J. D., St. Clair, J. M., Zhang,  
826 X., Schilling, K. A., Seinfeld, J. H., and Wennberg, P. O.: Isoprene NO<sub>3</sub> Oxidation Products from the  
827 RO<sub>2</sub> + HO<sub>2</sub> Pathway, *The Journal of Physical Chemistry A*, 10.1021/acs.jpca.5b06355, 2015.

828 Shao, Y., Gan, Z., Epifanovsky, E., Gilbert, A. T. B., Wormit, M., Kussmann, J., Lange, A. W., Behn,  
829 A., Deng, J., Feng, X., Ghosh, D., Goldey, M., Horn, P. R., Jacobson, L. D., Kaliman, I., Khaliullin, R.  
830 Z., Kuś, T., Landau, A., Liu, J., Proynov, E. I., Rhee, Y. M., Richard, R. M., Rohrdanz, M. A., Steele,  
831 R. P., Sundstrom, E. J., Woodcock, H. L., Zimmerman, P. M., Zuev, D., Albrecht, B., Alguire, E.,  
832 Austin, B., Beran, G. J. O., Bernard, Y. A., Berquist, E., Brandhorst, K., Bravaya, K. B., Brown, S. T.,  
833 Casanova, D., Chang, C.-M., Chen, Y., Chien, S. H., Closser, K. D., Crittenden, D. L., Diedenhofen,  
834 M., DiStasio, R. A., Do, H., Dutoi, A. D., Edgar, R. G., Fatehi, S., Fusti-Molnar, L., Ghysels, A.,  
835 Golubeva-Zadorozhnaya, A., Gomes, J., Hanson-Heine, M. W. D., Harbach, P. H. P., Hauser, A. W.,  
836 Hohenstein, E. G., Holden, Z. C., Jagau, T.-C., Ji, H., Kaduk, B., Khistyayev, K., Kim, J., Kim, J., King,  
837 R. A., Klunzinger, P., Kosenkov, D., Kowalczyk, T., Krauter, C. M., Lao, K. U., Laurent, A. D., Lawler,  
838 K. V., Levchenko, S. V., Lin, C. Y., Liu, F., Livshits, E., Lochan, R. C., Luenser, A., Manohar, P., Manzer,  
839 S. F., Mao, S.-P., Mardirossian, N., Marenich, A. V., Maurer, S. A., Mayhall, N. J., Neuscammen, E.,  
840 Oana, C. M., Olivares-Amaya, R., O'Neill, D. P., Parkhill, J. A., Perrine, T. M., Peverati, R., Prociuk,  
841 A., Rehn, D. R., Rosta, E., Russ, N. J., Sharada, S. M., Sharma, S., Small, D. W., Sodt, A., Stein, T.,  
842 Stück, D., Su, Y.-C., Thom, A. J. W., Tsuchimochi, T., Vanovschi, V., Vogt, L., Vydrov, O., Wang, T.,  
843 Watson, M. A., Wenzel, J., White, A., Williams, C. F., Yang, J., Yeganeh, S., Yost, S. R., You, Z.-Q.,  
844 Zhang, I. Y., Zhang, X., Zhao, Y., Brooks, B. R., Chan, G. K. L., Chipman, D. M., Cramer, C. J., Goddard,  
845 W. A., Gordon, M. S., Hehre, W. J., Klamt, A., Schaefer, H. F., Schmidt, M. W., Sherrill, C. D., Truhlar,  
846 D. G., Warshel, A., Xu, X., Aspuru-Guzik, A., Baer, R., Bell, A. T., Besley, N. A., Chai, J.-D., Dreuw,  
847 A., Dunietz, B. D., Furlani, T. R., Gwaltney, S. R., Hsu, C.-P., Jung, Y., Kong, J., Lambrecht, D. S.,  
848 Liang, W., Ochsenfeld, C., Rassolov, V. A., Slipchenko, L. V., Subotnik, J. E., Van Voorhis, T., Herbert,  
849 J. M., Krylov, A. I., Gill, P. M. W., and Head-Gordon, M.: Advances in molecular quantum chemistry  
850 contained in the Q-Chem 4 program package, *Molecular Physics*, 113, 184-215,  
851 10.1080/00268976.2014.952696, 2015.

852 Shepson, P. B., and Heicklen, J.: The wavelength and pressure dependence of the photolysis of  
853 propionaldehyde in air, *Journal of Photochemistry*, 19, 215-227, [http://dx.doi.org/10.1016/0047-](http://dx.doi.org/10.1016/0047-2670(82)80024-5)  
854 [2670\(82\)80024-5](http://dx.doi.org/10.1016/0047-2670(82)80024-5), 1982.

855 Shepson, P. B., Bottenheim, J. W., Hastie, D. R., and Venkatram, A.: Determination of the relative  
856 ozone and PAN deposition velocities at night, *Geophysical Research Letters*, 19, 1121-1124,  
857 10.1029/92GL01118, 1992.

858 Sprengnether, M., Demerjian, K. L., Donahue, N. M., and Anderson, J. G.: Product analysis of the  
859 OH oxidation of isoprene and 1,3-butadiene in the presence of NO, *Journal of Geophysical*  
860 *Research*, 107, 22437-22447, 10.1029/2001jd000716, 2002.

861 Starn, T. K., Shepson, P. B., Bertman, S. B., Riemer, D. D., Zika, R. G., and Olszyna, K.: Nighttime  
862 isoprene chemistry at an urban-impacted forest site, *Journal of Geophysical Research:*  
863 *Atmospheres*, 103, 22437-22447, 10.1029/98JD01201, 1998.

864 Su, L., Patton, E. G., Vilà-Guerau de Arellano, J., Guenther, A. B., Kaser, L., Yuan, B., Xiong, F.,  
865 Shepson, P. B., Zhang, L., Miller, D. O., Brune, W. H., Baumann, K., Edgerton, E., Weinheimer, A.,  
866 and Mak, J. E.: Understanding isoprene photo-oxidation using observations and modelling over a  
867 subtropical forest in the Southeast US, *Atmos. Chem. Phys. Discuss.*, 15, 31621-31663,  
868 10.5194/acpd-15-31621-2015, 2015.

869 Suarez-Bertoa, R., Picquet-Varrault, B., Tamas, W., Pangui, E., and Doussin, J. F.: Atmospheric fate  
870 of a series of carbonyl nitrates: photolysis frequencies and OH-oxidation rate constants,  
871 *Environmental science & technology*, 46, 12502-12509, 10.1021/es302613x, 2012.

872 Treacy, J., Hag, M. E., O'Farrell, D., and Sidebottom, H.: Reactions of Ozone with Unsaturated  
873 Organic Compounds, *Berichte der Bunsengesellschaft für physikalische Chemie*, 96, 422-427,  
874 10.1002/bbpc.19920960337, 1992.

875 Tuazon, E. C., Atkinson, R., Mac Leod, H., Biermann, H. W., Winer, A. M., Carter, W. P. L., and Pitts,  
876 J. N.: Yields of glyoxal and methylglyoxal from the nitrogen oxide(NOx)-air photooxidations of  
877 toluene and m- and p-xylene, *Environmental science & technology*, 18, 981-984,  
878 10.1021/es00130a017, 1984.

879 Tuazon, E. C., and Atkinson, R.: A product study of the gas-phase reaction of Isoprene with the  
880 OH radical in the presence of NOx, *International Journal of Chemical Kinetics*, 22, 1221-1236,  
881 10.1002/kin.550221202, 1990.

882 Vingarzan, R.: A review of surface ozone background levels and trends, *Atmospheric Environment*,  
883 38, 3431-3442, <http://dx.doi.org/10.1016/j.atmosenv.2004.03.030>, 2004.

884 Wang, X., Wang, T., Yan, C., Tham, Y. J., Xue, L., Xu, Z., and Zha, Q.: Large daytime signals of N2O5  
885 and NO3 inferred at 62 amu in a TD-CIMS: chemical interference or a real atmospheric  
886 phenomenon?, *Atmos. Meas. Tech.*, 7, 1-12, 10.5194/amt-7-1-2014, 2014.

887 Wiberg, K. B., Hadad, C. M., Rablen, P. R., and Cioslowski, J.: Substituent effects. 4. Nature of  
888 substituent effects at carbonyl groups, *Journal of the American Chemical Society*, 114, 8644-8654,  
889 10.1021/ja00048a044, 1992.

890 Wu, S., Mickley, L. J., Jacob, D. J., Logan, J. A., Yantosca, R. M., and Rind, D.: Why are there large  
891 differences between models in global budgets of tropospheric ozone?, *Journal of Geophysical*  
892 *Research: Atmospheres*, 112, D05302, 10.1029/2006JD007801, 2007.

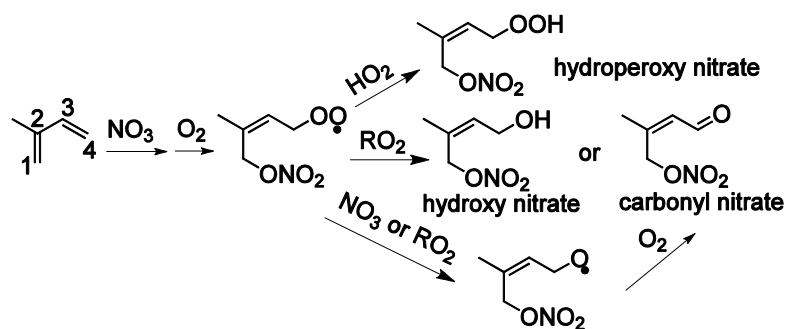
893 Xie, Y., Paulot, F., Carter, W. P. L., Nolte, C. G., Luecken, D. J., Hutzell, W. T., Wennberg, P. O.,  
894 Cohen, R. C., and Pinder, R. W.: Understanding the impact of recent advances in isoprene  
895 photooxidation on simulations of regional air quality, *Atmospheric Chemistry and Physics*, 13,  
896 8439-8455, 10.5194/acp-13-8439-2013, 2013.

897 Xiong, F., McAvey, K. M., Pratt, K. A., Groff, C. J., Hostetler, M. A., Lipton, M. A., Starn, T. K., Seeley,  
898 J. V., Bertman, S. B., Teng, A. P., Crouse, J. D., Nguyen, T. B., Wennberg, P. O., Misztal, P. K.,  
899 Goldstein, A. H., Guenther, A. B., Koss, A. R., Olson, K. F., de Gouw, J. A., Baumann, K., Edgerton,  
900 E. S., Feiner, P. A., Zhang, L., Miller, D. O., Brune, W. H., and Shepson, P. B.: Observation of  
901 isoprene hydroxynitrates in the southeastern United States and implications for the fate of NOx,  
902 *Atmos. Chem. Phys.*, 15, 11257-11272, 10.5194/acp-15-11257-2015, 2015.

903 Zellner, R., and Lorenz, K.: Laser photolysis/resonance fluorescence study of the rate constants  
904 for the reactions of hydroxyl radicals with ethene and propene, *The Journal of Physical Chemistry*,  
905 88, 984-989, 10.1021/j150649a028, 1984.

906

907

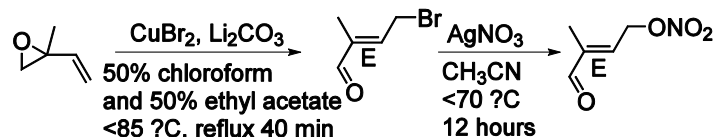


908

909 Figure 1. Organic nitrates produced from  $\text{NO}_3$ -initiated isoprene oxidation.

910

911



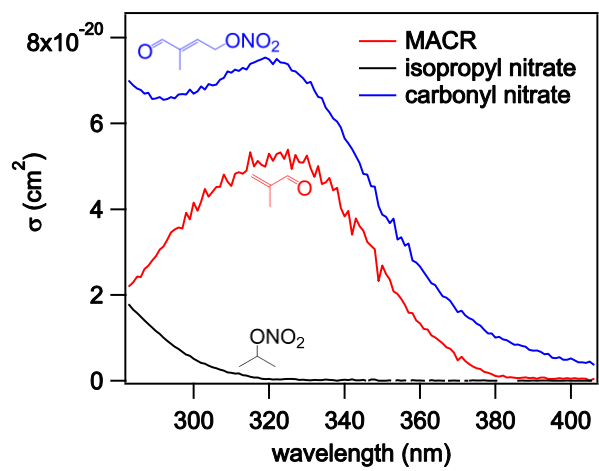
912

913

914 Figure 2. The synthesis route for the 4,1-isoprene carbonyl nitrate/nitrooxy enal.

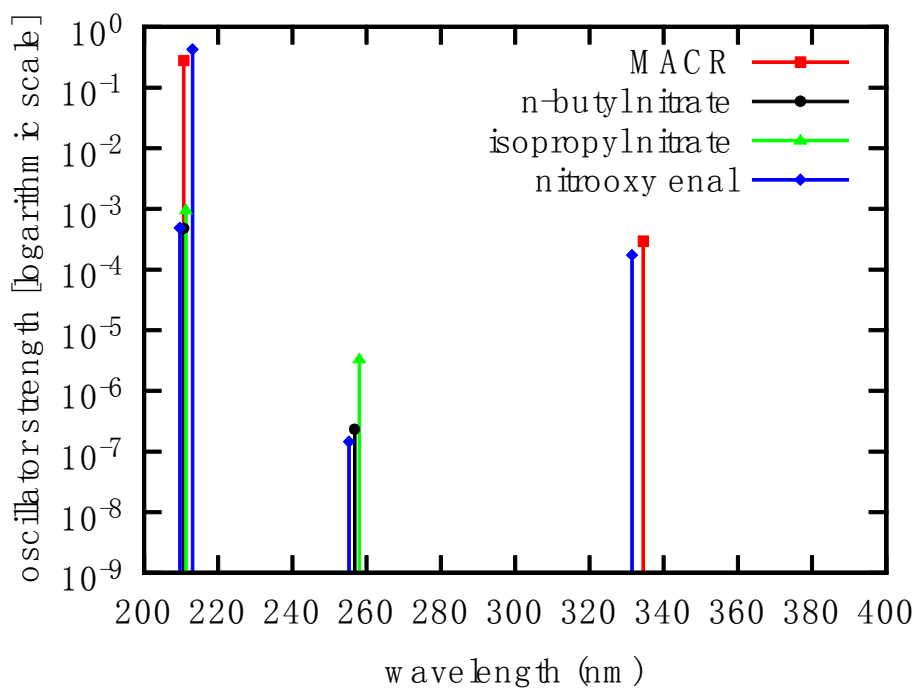
915

916



917  
 918  
 919 Figure 3. UV absorption cross section of the ~~carbonyl nitrate~~nitrooxy enal, MACR and isopropyl  
 920 nitrate. The spectra were all obtained in acetonitrile solvent.  
 921  
 922

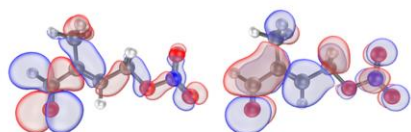




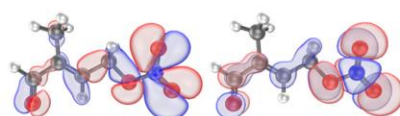
Formatted: Font: (Default) Arial

923  
 924  
 925 Figure 4. Theoretical gas-phase absorption spectra of the carbonyl nitrate nitrooxy enal, MACR,  
 926 isopropyl nitrate and *n*-butyl nitrate in the gas phase.  
 927  
 928

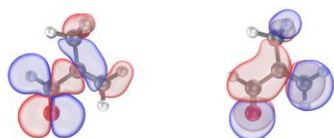
(a) First excitation in nitrooxy enal  
331.51 nm  $\approx$  3.7404 eV  
HOMO  $\rightarrow$  LUMO



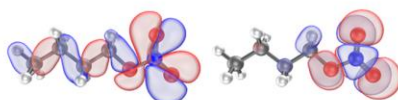
(b) Second excitation in nitrooxy enal  
255.27 nm  $\approx$  4.8575 eV  
HOMO-2  $\rightarrow$  LUMO+1



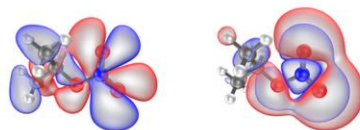
Homologous excitation in MACR  
334.54 nm  $\approx$  3.7066 eV  
HOMO  $\rightarrow$  LUMO



Homologous excitation in *n*-butyl nitrate  
256.76 nm  $\approx$  4.8295 eV  
HOMO  $\rightarrow$  LUMO

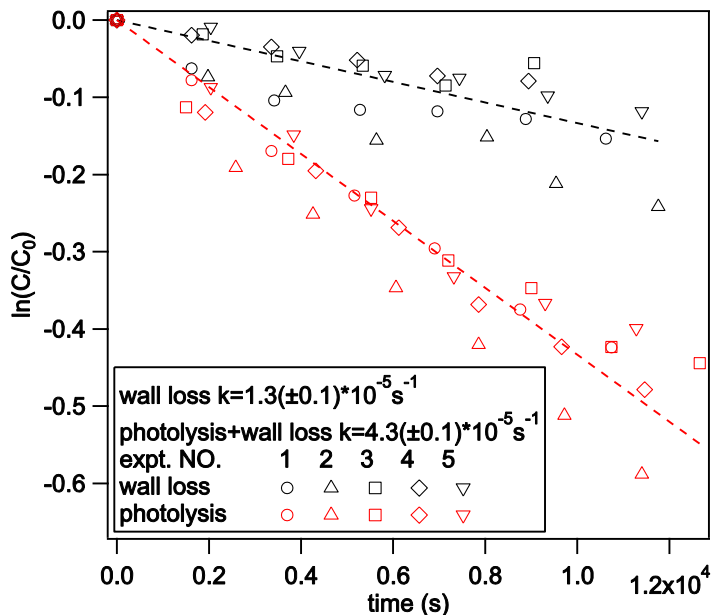


Homologous excitation in isopropyl nitrate  
258.02 nm  $\approx$  4.8058 eV  
HOMO  $\rightarrow$  LUMO



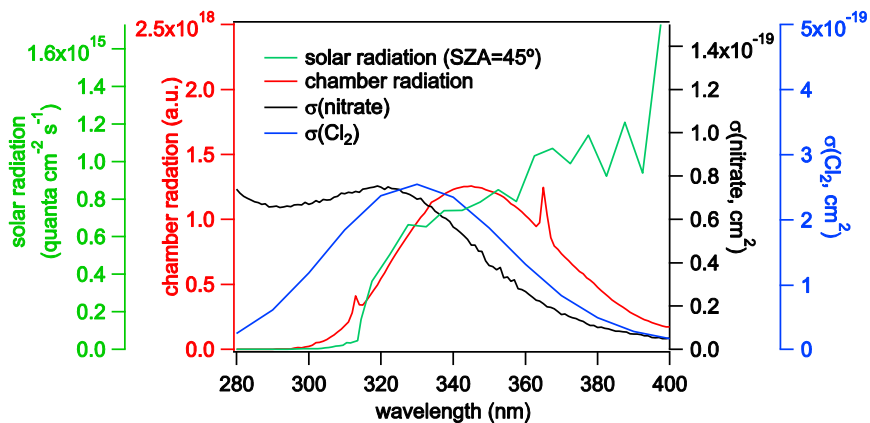
929  
930  
931  
932  
933  
934  
935

Figure 5. Molecular orbital analysis of the first (a) and second (b) electronic excitations of the ~~carbonyl nitrate~~ nitrooxy enal, along with analogous excitations of MACR, isopropyl nitrate and *n*-butyl nitrate. The blue and red colors represent the opposite phases of molecular orbitals.



936  
937  
938  
939  
940  
941

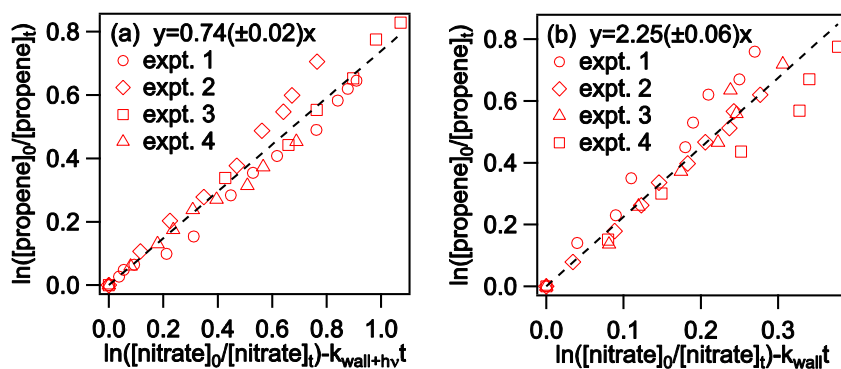
Figure 6. Wall loss and photolysis loss of the carbonyl nitrate nitrooxy enal in the reaction chamber.



942  
943  
944  
945  
946

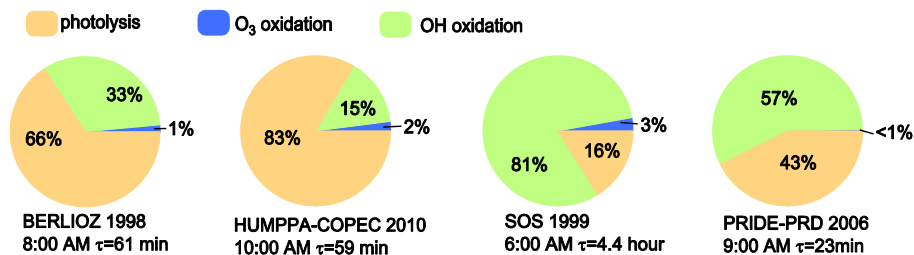
Figure 7. The radiation spectra of the chamber (red) and the sun (green, SZ A=45° as an example), and the absorption spectra of the carbonyl nitrate nitrooxy enal (black, obtained in the liquid phase using acetonitrile solvent) and chlorine (blue).

947  
948  
949



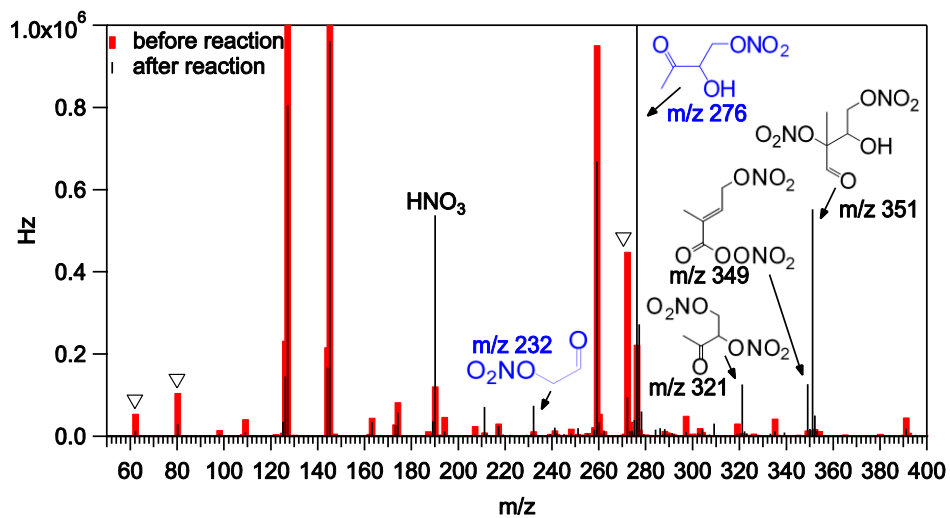
950  
951  
952  
953  
954  
955  
956

Figure 8. The first-order loss of propene relative to that of the carbonyl nitrate for OH-initiated (a) and O<sub>3</sub>-initiated (b) oxidation reactions.



957  
958  
959  
960  
961  
962  
963  
964  
965  
966

Figure 9. The relative contributions of photolysis (orange), OH oxidation (green) and O<sub>3</sub> oxidation (blue) to the photochemical decay of the carbonyl nitrate, calculated based on measured OH and O<sub>3</sub> concentrations for the following field studies: BERLIOZ 1998 study at Pabstthum, Germany (Mihelcic et al., 2003; Platt et al., 2002), HUMPPA-COPEC 2010 study at Hyytiälä (Hens et al., 2014), Finland, SOS 1999 study at Nashville, US (Martinez et al., 2003; Roberts et al., 2002) and PRIDE-PRD 2006 study at Guangzhou, China (Lu et al., 2012).



967  
968  
969  
970  
971  
972  
973  
974  
975  
976

Figure 10. The CIMS spectra before (red) and after (black) the OH + carbonyl nitrate nitrooxy enal oxidation reaction. The inverted triangles show the decreases in CIMS signals for the carbonyl nitrate nitrooxy enal (m/z 272) and the NO<sub>3</sub><sup>-</sup> fragments (m/z 62, water cluster at m/z 80) derived from the carbonyl nitrate (Fig. 11). The molecular structures are inferred from the nominal masses observed by CIMS. The compounds that were observed by both CIMS and GC (Fig. 13) are colored in blue.



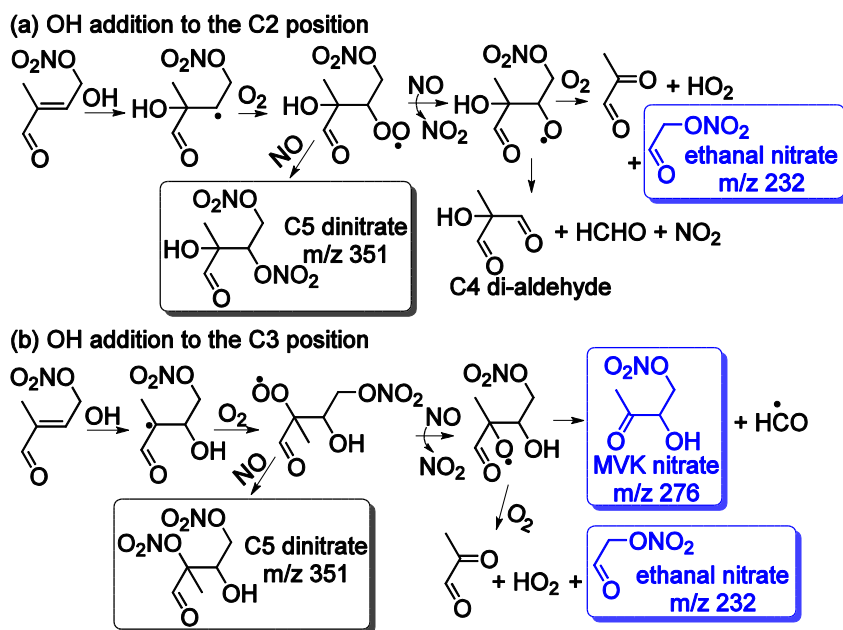
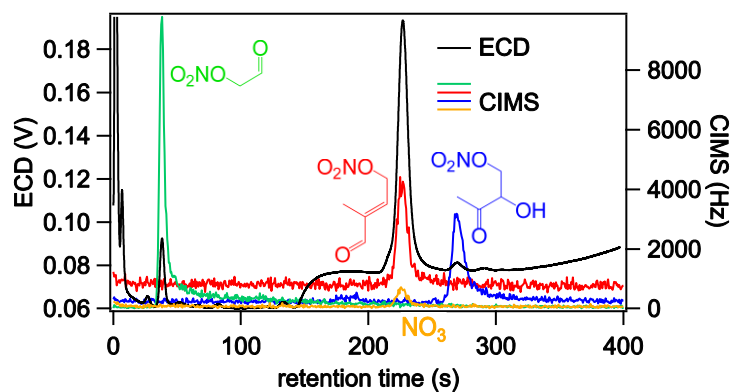
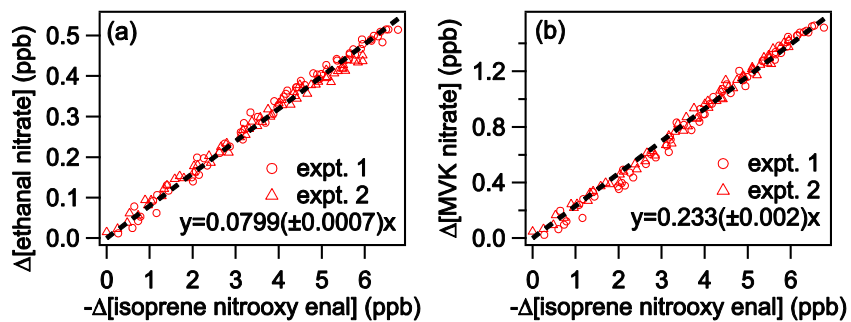


Figure 12. Proposed reaction mechanisms for OH addition to the C2 (a) and C3 (b) position of the carbonyl nitrate/nitrooxy enal. The compounds in boxes are proposed products inferred from the nominal masses observed by the CIMS (Fig. 8). The compounds that were observed by both CIMS and GC (Fig. 13) are colored in blue.

986  
987  
988  
989  
990  
991  
992  
993  
994  
995  
996

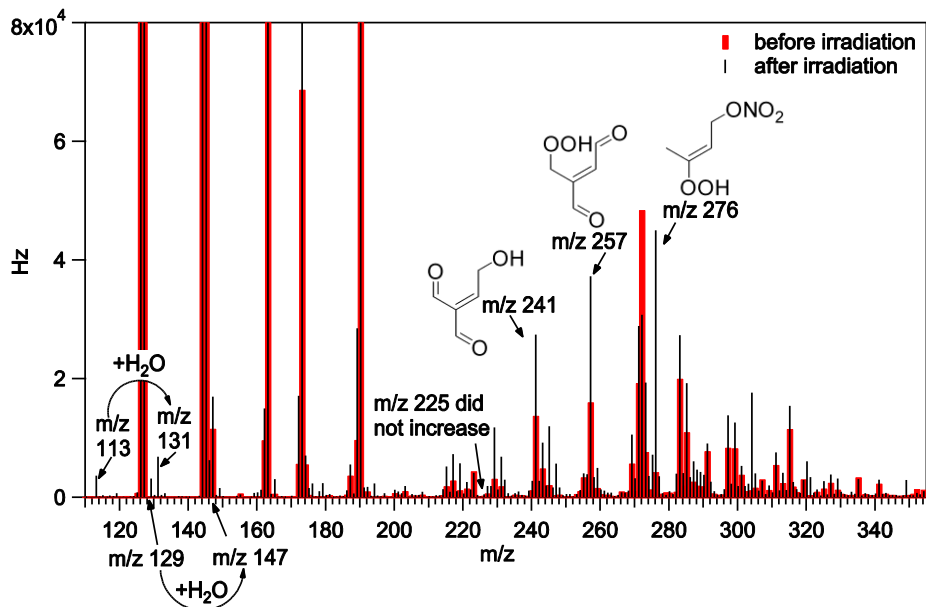


997  
998 Figure 13. The GC-ECD/CIMS spectra for the ~~carbonyl nitrate~~nitrooxy enal (red), MVK nitrate  
999 (blue) and ethanal nitrate (green). The reaction of iodide with the ~~carbonyl nitrate~~nitrooxy enal  
1000 generated  $\text{NO}_3^-$  ion (orange). The ECD chromatogram is shown in black.  
1001  
1002

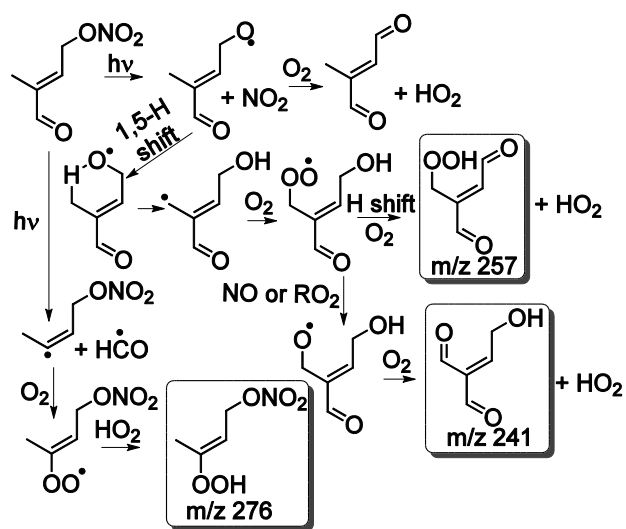


1003  
1004  
1005 Figure 14. The formation of ethanal nitrate (a) and MVK nitrate (b) relative to the loss of the  
1006 isoprene ~~carbonyl nitrate~~nitrooxy enal for the OH + ~~carbonyl nitrate~~nitrooxy enal oxidation  
1007 experiments.  
1008  
1009





1010  
 1011 Figure 15. CIMS spectra before (red) and after (black) the photolysis of the isoprene ~~carbonyl~~  
 1012 ~~nitrate~~ nitrooxy enal. The molecular structures are inferred from the nominal masses observed by  
 1013 CIMS.  
 1014  
 1015  
 1016



1017  
 1018 Figure 16. A proposed reaction mechanisms for the carbonyl-nitrate-nitrooxy enal photolysis  
 1019 reaction. The compounds in boxes are proposed products as inferred from nominal masses observed  
 1020 by the CIMS (Fig. 13).  
 1021